"COMPOSITE CERAMIC SUPERCONDUCTING WIRES FOR ELECTRIC MOTOR APPLICATIONS"

(1)

PRIME CONTRACTOR

CPS SUPERCONDUCTOR CORPORATION
A Subsidiary of
Ceramics Process Systems Corporation
155 Fortune Boulevard
Milford, Massachusetts 01757

December 31, 1990

DARPA Order Number: 9525
Contract Number: N00014-88-C-0512
Contract Effective Date: June 30, 1988
Contract Expiration Date: September 30, 1991
Principal Investigator: Mark V. Parish, Ph.D.
(508) 634-3422

Prepared for:

Defense Advanced Research Projects Agency
1400 Wilson Boulevard
Arlington, VA 22209

Office of Naval Research
800 North Quincy Street
Arlington, VA 22217

APPROVED FOR PUBLIC RELEASE: DISTRIBUTION IS UNLIMITED

CPS SUPERCONDUCTOR
CORPORATION

TENTH QUARTERLY REPORT

FOR THE PROJECT

"COMPOSITE CERAMIC SUPERCONDUCTING WIRES FOR ELECTRIC MOTOR APPLICATIONS"

PRIME CONTRACTOR

CPS SUPERCONDUCTOR CORPORATION
A Subsidiary of
Ceramics Process Systems Corporation
155 Fortune Boulevard
Milford, Massachusetts 01757

December 31, 1990

DARPA Order Number: 9525
Contract Number: N00014-88-C-0512
Contract Effective Date: June 30, 1988
Contract Expiration Date: September 30, 1991
Principal Investigator: Mark V. Parish, Ph.D.
(508) 634-3422

Prepared for:

Defense Advanced Research Projects Agency
1400 Wilson Boulevard
Arlington, VA 22209

Office of Naval Research
800 North Quincy Street
Arlington, VA 22217

REPORT DOCUMENTATION PAGE

Form Approved
OMB No. 0704-0188

1. AGENCY USE ONLY (Leave blank)	2. REPORT DATE	3. REPORT TYPE AND DATES COVERED
	12-31-90	Technical Report 10-1-90 thru. 12-31-90

4. TITLE AND SUBTITLE
Composite Ceramic Superconducting Wires for Electric Motor Applications

5. FUNDING NUMBERS
N00014-88-C-0512

6. AUTHOR(S)
DR. MARK V. PARISH

7. PERFORMING ORGANIZATION NAME(S) AND ADDRESS(ES)
CPS SUPERCONDUCTOR CORPORATION
155 Fortune Boulevard
Milford, MA 01757

8. PERFORMING ORGANIZATION REPORT NUMBER
CPSS-1290-01

9. SPONSORING/MONITORING AGENCY NAME(S) AND ADDRESS(ES)
Defense Advanced Research Projects Agency
1400 Wilson Boulevard, Arlington, VA 22209

Office of Naval Research
800 North Quincy Street, Arlington, VA 22217-500

10. SPONSORING/MONITORING AGENCY REPORT NUMBER

11. SUPPLEMENTARY NOTES
N/A

12a. DISTRIBUTION/AVAILABILITY STATEMENT
Unlimited

12b. DISTRIBUTION CODE

13. ABSTRACT (Maximum 200 words)

A process for producing technologically useful HTSC wire for application in a prototype HTSC electric motor is proceeding. Activities include: 1) Melt-textured $YBa_2Cu_3O_{7-\delta}$ fiber, 2) Melt-textured $YBa_2Cu_3O_{7-\delta}$ disks and shapes, and 3) $Bi_2Ca_2Sr_2Cu_3O_{10}$ fiber. Our attempts to melt-texture $YBa_2Cu_3O_{7-\delta}$ fiber and wire have continued to be very successful. Fibers have been produced that show a transport J_c of 20,000 A/cm^2 in self field at 77 K. These fibers are produced continuously and lengths of up to 1.0 meter have been successfully textured. Work this past quarter has advanced our understanding of the relationship between processing conditions, microstructure, electrical characteristics, and improvements in fiber uniformity. BiSCCO ribbon wire was further developed. The development of a robust process for producing a reproducible BiSCCO powder for use as process feedstock have been defined this quarter. Emerson Electric has designed, constructed, and tested the brushless "trapped magnetic flux permanent magnet" motor. Essentially a permanent magnet motor where melt-textured $YBa_2Cu_3O_{7-\delta}$ magnet "replicas" are used is awaiting the test results of $YBa_2Cu_3O_{7-\delta}$ magnet replicas.

14. SUBJECT TERMS	15. NUMBER OF PAGES
Superconductor, ceramic, motor	52
	16. PRICE CODE

17. SECURITY CLASSIFICATION OF REPORT	18. SECURITY CLASSIFICATION OF THIS PAGE	19. SECURITY CLASSIFICATION OF ABSTRACT	20. LIMITATION OF ABSTRACT
Unclassified	Unclassified	Unclassified	

EXECUTIVE SUMMARY

On December 10, 1990, the CPS DARPA II contract was extended six months through the end of DARPA FY91 (September 30, 1991) with the original FY91 allocation of $1.3MM. Our program has been scaled and focused accordingly. A revised plan that succeeds the changes effective August 2, 1990,[1] discussed in the last quarterly report, will be reviewed with the contract and scientific officers early in January, 1991. The major modifications to the program are stated in this report.

This report describes progress on the development of a process for producing technologically useful HTSC wire for application in a prototype HTSC electric motor. A primarily focus has been on the improvement of the critical current density of melt-textured $YBa_2Cu_3O_{7-\delta}$ fiber/wire to yield high J_c wire. Our technical efforts during Quarter 10 have focussed on materials and process developments aimed at producing high critical current, weak-link free superconductors. These activities include: 1) Melt-textured $YBa_2Cu_3O_{7-\delta}$ fiber, 2) Melt-textured $YBa_2Cu_3O_{7-\delta}$ disks and shapes, and 3) $Bi_2Ca_2Sr_2Cu_3O_{10}$ fiber. The program and funding extension narrows our work to two major areas effective December 11, 1990, each aimed at developing only 77 K bulk HTSC's, i.e., $YBa_2Cu_3O_{7-\delta}$. The primary activity will be to further develop our melt-textured $YBa_2Cu_3O_{7-\delta}$ fiber process; the secondary activity has two distinct tasks--production of melt-textured $YBa_2Cu_3O_{7-\delta}$ disks and melt-textured shapes (rings), both for use in the "trap flux" motor.

Our attempts to melt-texture $YBa_2Cu_3O_{7-\delta}$ fiber and wire have continued to be very successful. Fibers have been produced that show a transport J_c of 20,000 A/cm^2 in self field at 77 K. These fibers are produced continuously and lengths of up to 1.0 meter have been successfully textured. Work this past quarter has advanced our understanding of the relationship between processing conditions, microstructure, electrical characteristics, and improvements in fiber uniformity.

BiSCCO ribbon wire was further developed. The development of a robust process for producing a reproducible BiSCCO powder for use as process feedstock have been defined this quarter. Due to the refocussing of the overall program efforts, BiSCCO powder development and wire production have, consequently, been removed from this DARPA program.

Work has proceeded by Emerson Electric on the design, construction, and testing of a brushless "trapped magnetic flux permanent magnet" motor. This design, essentially a permanent magnet motor where melt-textured $YBa_2Cu_3O_{7-\delta}$ magnet "replicas" are used in place of conventional magnets, has been fabricated and tested, and is presently awaiting the test results of $YBa_2Cu_3O_{7-\delta}$ magnet replicas.

---

[1] Letter to F. Patten dated August 6, 1990, confirming agreed upon changes at August 2, 1990 meeting.

TABLE OF CONTENTS

LIST OF FIGURES

COMPOSITE CERAMIC SUPERCONDUCTING WIRES FOR ELECTRIC MOTOR APPLICATIONS

Mark V. Parish, Ph.D.
Principal Investigator
CPS Superconductor Corporation
Milford, MA 01757

1. PROGRAM SUMMARY

This Tenth Quarterly Report covers activities during October through December 1990 on a program aimed at the development of high temperature superconducting (HTSC) wire and the utilization of this wire in a prototype superconducting motor. The program is being carried out by CPS Superconductor Corporation, a subsidiary of Ceramics Process Systems Corporation, responsible for wire and materials development, and two subcontractors: Albany International Research Corporation (AIResCo), responsible for development and production of green fibers and fiber assemblies, and the Emerson Motor Division (EMD) of Emerson Electric, for the design and construction of the program's HTSC motors.

2. PROGRAM STATUS

This quarter has proceeded with further implementation of processes to improve the electrical behavior our HTSC wire. Efforts in the areas of melt-texturing of $YBa_2Cu_3O_{7-\delta}$ fibers and wires have been emphasized and considerable progress is continually being made. Due to refocusing of our efforts near the end of Quarter 10, BiSCCO powder development and mechanical texturing of $Bi_2Ca_2Sr_2Cu_3O_{10}$ wires were terminated as part of this DARPA program. The effort at EMD has continued to

develop the "trapped-flux" motor design, and has commenced testing of present melt-textured HTSC materials.

The status of the program is compared with individual tasks of the revised Statement of Work in Figures 2.1, 2.2, and 2.3 that show timelines for the major fiber, wire and motor development tasks, respectively. The fiber spinning tasks, as shown, involved both $YBa_2Cu_3O_{7-\delta}$ and $Bi_2Ca_2Sr_2Cu_3O_{10}$ melt spinning and braiding. The wire tasks show several changes; the main effort is now melt-texturing monofilament wire, with braided multifilamentary wire as a possible secondary effort and the postponement of the BiSCCO work. The emphasis within the motor task is production of a "trapped-flux" motor, using the capabilities of present HTSC technology.

The following sections detail the program's progress. Section 2.1 covers efforts in raw material (powder) synthesis and production conducted at CPS Superconductor. Section 2.2 details the fiber spinning work conducted at Albany International Research Corporation in Mansfield, Massachusetts. Section 2.3 describes wire and fiber cladding, sintering/thermal processing, and characterization work conducted at CPS Superconductor. Section 2.4 outlines the HTSC motor activities at Emerson Motor Division.

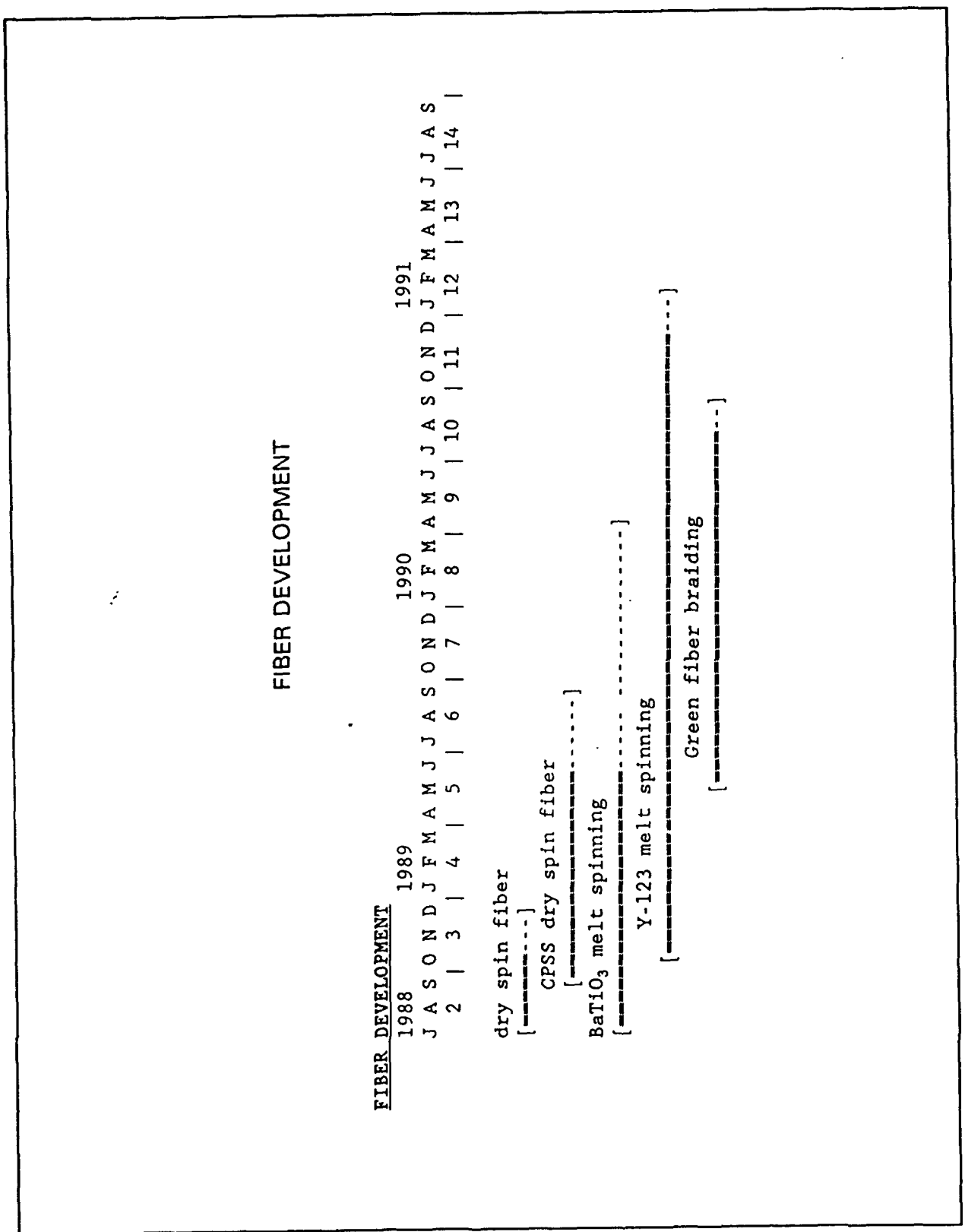

Figure 2.1 Revised Project Schedule for Fiber Tasks.

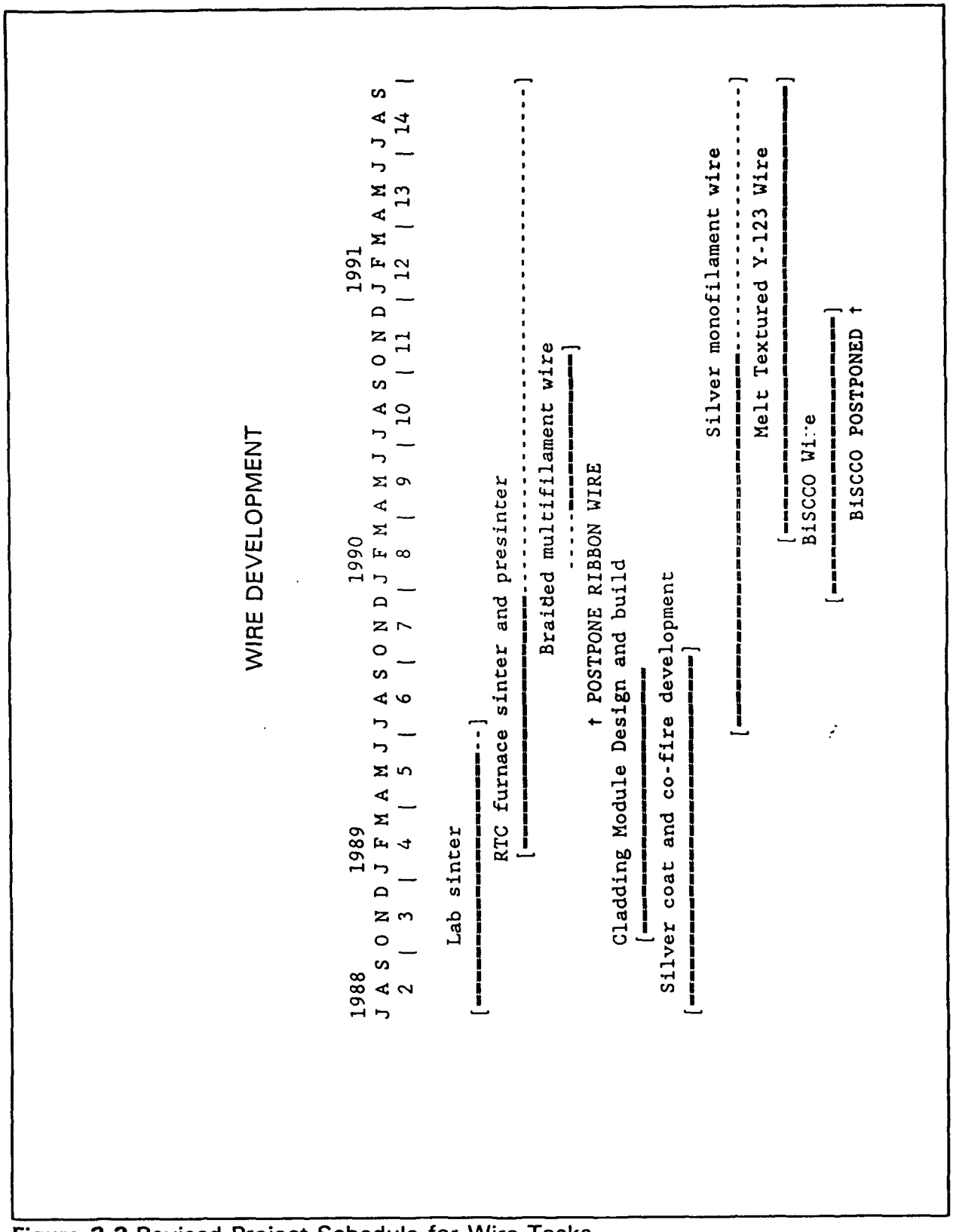

Figure 2.2 Revised Project Schedule for Wire Tasks.

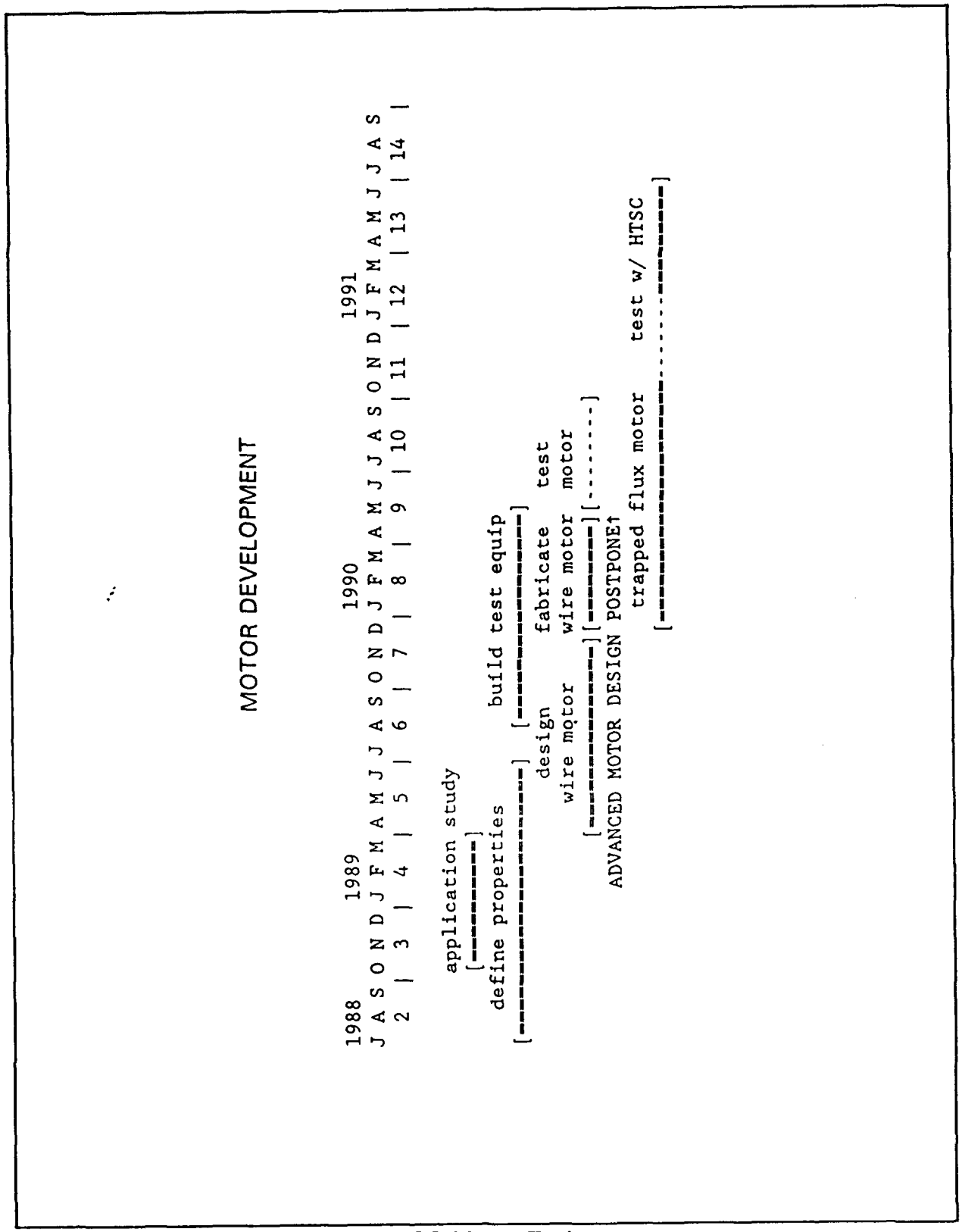

Figure 2.3 Project Schedule for HTSC Motor Tasks.

2.1 Raw Materials Synthesis and Production

L.J. Klemptner, Hyun D. Park, and D. Gobielle
CPS Superconductor Corporation

Quarter 10 has recognized steady activities in the area of materials development work of $YBa_2Cu_3O_{7-\delta}$. Greater effort has been placed on the synthesis of off-stoichiometric and rare earth-substituted $YBa_2Cu_3O_{7-\delta}$ compositions. Materials development work in the BiSCCO area was advanced before being temporarily terminated in mid-December.

2.1.1. Off-Stoichiometric and Substituted $YBa_2Cu_3O_{7-\delta}$

Work on melt-texturing presents the need for a wider variety of YBCO-based compositions. In this quarter, we produced mixtures of $YBa_2Cu_3O_{7-\delta}$ and Y_2BaCuO_5 (211) and Ag_2O, and a rare-earth substituted $YBa_2Cu_3O_{7-\delta}$ compound, $NdBa_2Cu_3O_{7-\delta}$, to support our melt-texturing efforts. These compounds were produced for use initially in disk tests, and eventually for fiber spinning, necessitating production in kilogram quantities.

Mixtures of 211 and $YBa_2Cu_3O_{7-\delta}$ were produced by blending appropriate amounts of the prereacted components allowing the greatest phase control, as described in the last quarterly report. The 211 required for these vibro-milled mixtures was made in-house using a modification of the proprietary CPS Superconductor $YBa_2Cu_3O_{7-\delta}$ synthesis method. Batches of 7.5 (3.2 kg), 15 (1.6 kg), 20 (400 g), 30 (300 g), and 40 (300 g) wt% 211 were produced.

Rare-earth substituted 123 compounds continued to be developed for the CPS Superconductor melt-texturing studies, involving substitution of the appropriate rare earth oxide (e.g., Nd_2O_3) for Y_2O_3 starting material in the CPS Superconductor powder process. To date, neodymium-substituted compounds have been batched and calcined; grinding is necessary before disks are tested and fibers are spun.

In addition, 300 g of 20 wt% 211, 5% Ag_2O was prepared for melt-texturing experiments.

2.1.2. $Bi_2Ca_2Sr_2Cu_3O_{10}$ Powder Synthesis

A process for producing BiSCCO powder at CPS Superconductor was modeled after our $YBa_2Cu_3O_{7-\delta}$ process, using inexpensive, mechanically mixed oxides capable of economical scale-up to kilogram production levels. The high T_c, lead-doped 2223 BiSCCO composition was selected based on a literature survey. Using a modification of our fiber spinning/continuous firing process, we intended to investigate the possibility of minimizing or eliminating the final, lengthy annealing step routinely used to convert the low T_c 2212 BiSCCO to 2223 BiSCCO. The development work investigated three fundamental variables: stoichiometry (Pb/Bi ratios, excess Ca and Cu, and a number of minor dopants), calcining atmosphere, and calcination time and temperature. The goal was to maximize the 2223 phase while minimizing the calcination time as was previously reported in the last quarterly report.

Three viable compositions, BP5 ($Bi_{1.2}Pb_{0.8}Ca_2Sr_2Cu_3O_{10}$), BPH5 (a barium, magnesium doped form of BP5), and BPH2 ($Bi_{1.7}Pb_{0.3}Ca_2Sr_2Cu_3O_{10}$) were prepared enabling us to refine our processing conditions to produce 3 kg of each material with

a high fraction of 2223. As reported last quarter, precursor powders are initially calcined at 775°C for 6 hours, followed by an extended heating at 830 to 850°C for periods between 30 and 120 hours in air/nitrogen mixtures. The formation of 2223 at 830°C is initially very rapid, approximately 90% 2223 after 30 h, then slows considerably, reaching only 95% 2223 after a 90 h calcination.

The estimates of high T_c versus the low T_c phase contents (2223 versus 2212) that determine 2223-BiSCCO powder quality noted for the above powders were determined by relative peak heights of characteristic major peaks in X-ray diffraction patterns. In an attempt to verify these data, experiments were performed to understand the relationship between magnetic volume susceptibility (based on magnetic shielding) and the X-ray diffraction pattern's relative peak heights. Figure 2.4 (a. through e.) shows a series of results of full scale (0-60 degrees, two-theta) X-ray diffraction patterns, enlarged areas from two-theta 0 to 7 degrees of the same X-ray diffraction data, and the corresponding volume susceptibility for various powders: a) a small hand-processed lot BPH2 powder, b) a production lot BPH2 powder, c) another production lot BPH2 powder that was removed from the process in the agglomerate stage, before grinding, d) a hand-processed lot BP5 powder, and e) a production lot BPH5 powder.

Several inconsistencies are evident when the high and low T_c phase contents are estimated by the X-ray diffraction pattern peak heights (referred to as the XRD

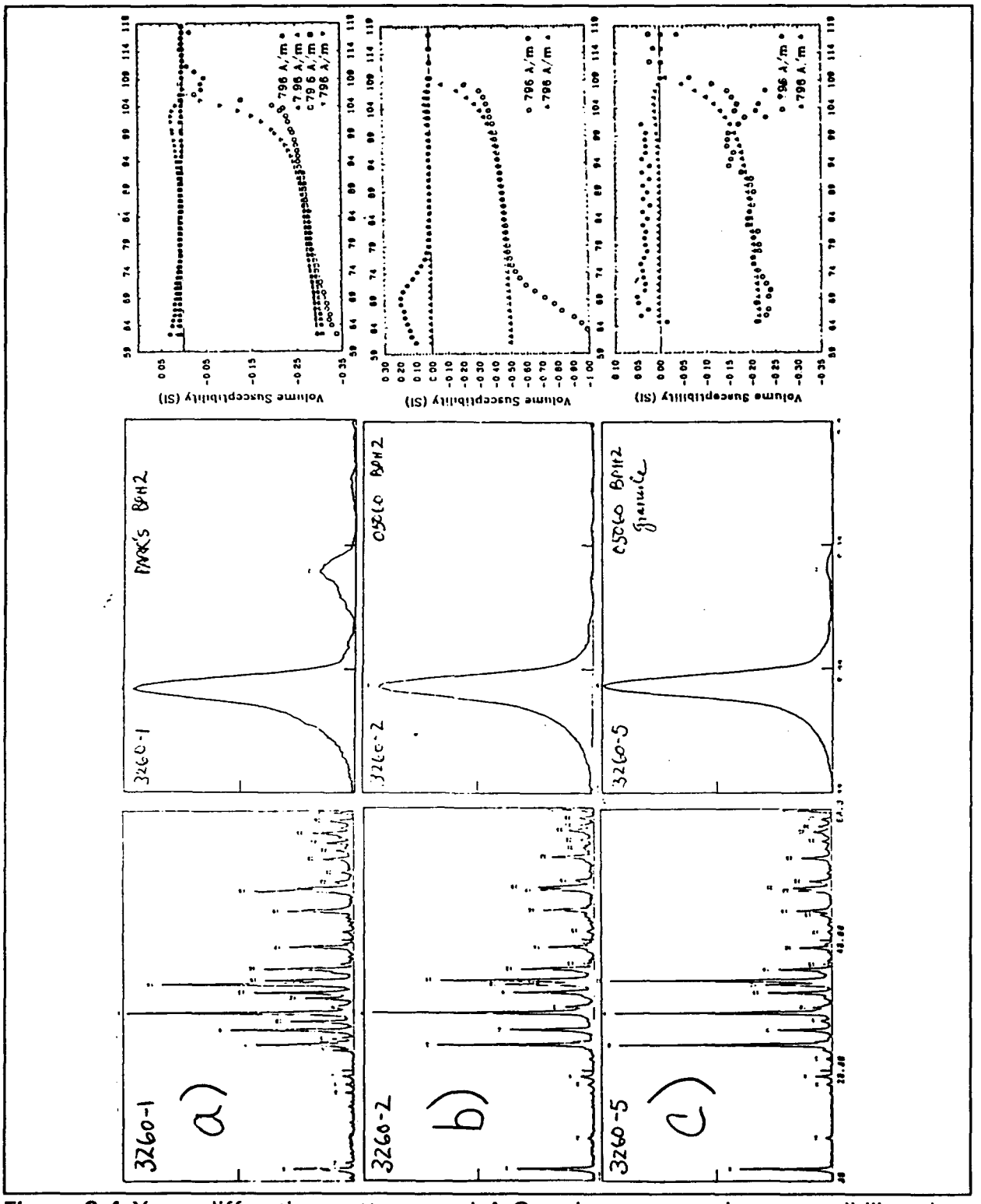

Figure 2.4 X-ray diffraction patterns and A.C. volume magnetic susceptibility plots for various BiSCCO powders: a) a small hand processed lot BPH2, b) a production lot BPH2, and c) a production lot BPH2 sample in the pre-ground agglomerate stage.

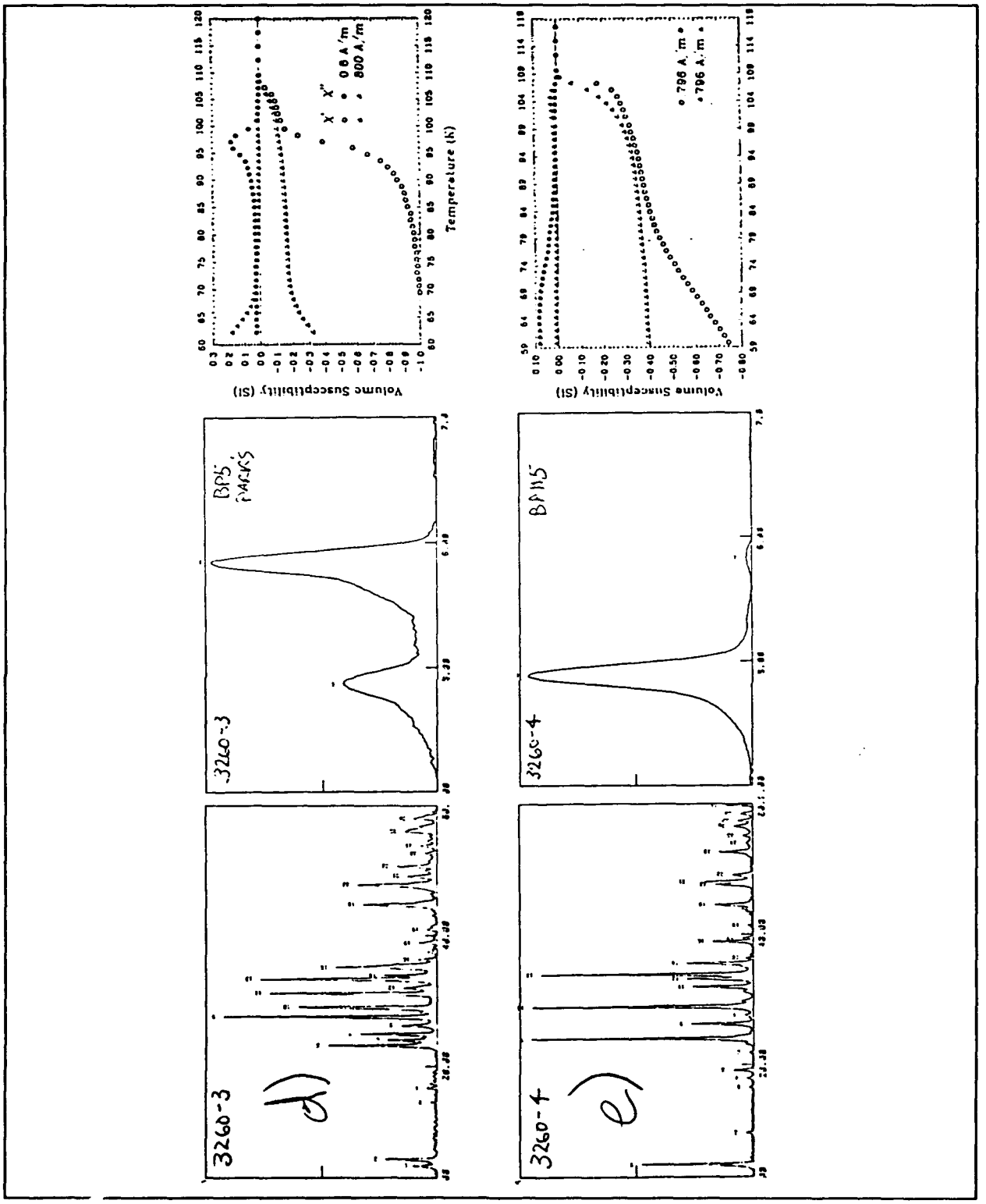

Figure 2.4 (con't) X-ray diffraction patterns and volume magnetic susceptibility plots for various BiSCCO powders: d) a hand processed lot BPH5, and e) a production lot BPH5.

method here)[2] or by the volume magnetic susceptibility (VMS method) data, though they may be explained. For example, note that the XRD method for the calcined agglomerates sample in Figure 2.4 c) clearly shows >90% 2223 phase, but the corresponding VMS method showed <25% shielding by the high T_c phase, and no evidence of the low T_c phase. In contrast, the example shown in Figure 2.4 d) showed evidence of only ~35% 2223 phase by XRD, whereas the VMS method shows 100% 2223 phase shielding. Perhaps, the combination of two phenomena could explain these data. First, the VMS samples may contain 2212-BiSCCO phase particles that are transforming to 2223 phase on their outer surface. The resulting volume susceptibility with temperature curves would show only the high T_c 2223-BiSCCO phase, since the 2212 phase would be "shielded" from detection. Under a small applied magnetic field, the amount of high T_c phase usually shows a decrease in the fraction of magnetic susceptibility (the two curves plotted in the VMS results) because of weak-links between the particles or grains. However, the XRD samples are prepared by grinding the powders. If the low T_c phase is contained in a high T_c "shell," grinding would expose the low T_c phase so that an intensity peak would display on the XRD plot.

In conclusion, the XRD method seems to be a better indicator of the phase quality of the BiSCCO powders, though magnetic susceptibility should be used to compliment the results. In addition, the modified powder process used to produce

---

[2] The high T_c 2223-BiSCCO phase displays a peak near the two-theta value of 5 degrees, whereas the low T_c 2212-BiSCCO phase displays a peak near 6 degrees.

these powders result in high-phase-pure products, even preferable over the small-lab-top produced samples. For example, the X-ray diffraction pattern in Figure 2.4. e) is representative of CPS Superconductor's 2223-BiSCCO powder calcined at 830°C for 60 hours. As can be observed, our production method yields high quality, high T_c phase 2223-BiSCCO in large kilogram size lots.

Samples of Hoechst-Celanese BiSCCO-2223 and $YBa_2Cu_3O_{7-\delta}$ were analyzed as possible sources of raw materials to be substituted into our process. The 2223 phase content in the Hoechst-Celanese BiSCCO was lower than our own (~80% as compared to our >95%), and though the phase purity of their $YBa_2Cu_3O_{7-\delta}$ was high, the surface area was too low, less than 2 m^2/g (i.e., particle size too large) than our process requires (>2 mg^2/g or <1.2 μm average). Other BiSCCO-2223 and -2212 samples were obtained from SSC for the same evaluation. Again, the phase content of 2223 was much lower than in the "2223" powder that we produce.

Fibers were spun from one batch of BPH5-(~75%)2223 BiSCCO powder with diameters of 5 and 10 μm. Most of a ten meter sample of the 10 μm fiber was coated with a thick layer of silver particles, cofired, mechanically rolled, annealed and tested for transport conductivity and magnetic susceptibility using a method explained in detail in the last quarterly report. Though the results were not striking, they showed promise. Figure 2.5 shows SEM micrographs of a silver clad, cofired and rolled BiSCCO wire sample, the silver evident in the left micrograph displaying its ductile fracture morphology. It is apparent that the plate-like particles are not as well aligned as was intended. More work is necessary in the rolling and annealing steps

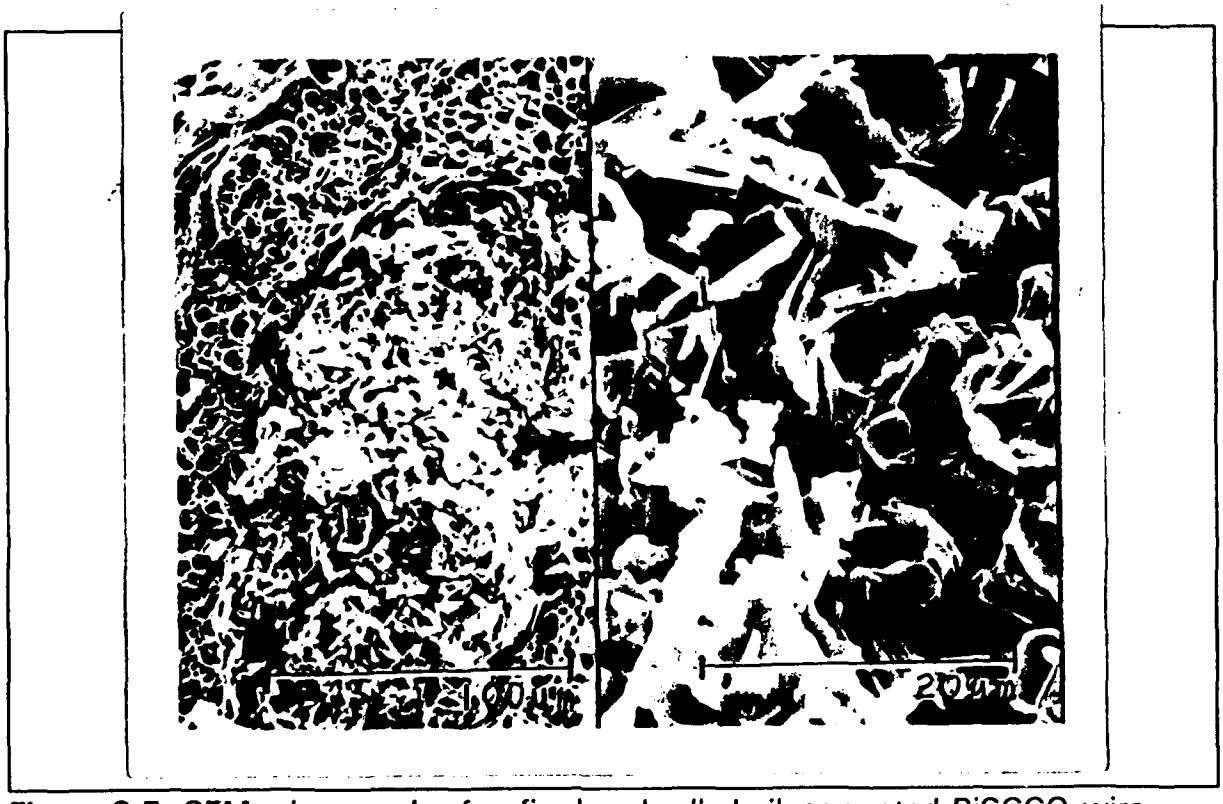

Figure 2.5. SEM micrograph of cofired and rolled silver coated BiSCCO wire.

to produce a more favorable microstructure. However, the sintered silver layer did perform well, not displaying cracks or areas where a liquid phase could escape during the annealing step. Other promising evidence to support this process can be seen in Figure 2.6 where the volume susceptibility of the sintered BiSCCO wire sample at shows that the high T_c phase still remains after the wire processing. The shifting of the curve in the small applied magnetic field indicates that the current path is weak-linked, as expected due to the microstructure. There was a small superconducting transport current measured in the bare section of the processed wire as indicated in Figure 2.7, though the silver clad cofired section did not exhibit a superconducting transport path. Again, more work is needed to optimize the rolling and annealing stages of the process.

2.1.3. $YBa_2Cu_3O_{7-\delta}$ Powder Synthesis

The bulk of the raw material produced at CPS Superconductor is $YBa_2Cu_3O_{7-\delta}$. Due to improvements in the powder process reported last quarter, the phase and chemical purity of the fine particle size material produced to date have proven more than adequate for any foreseeable processing needs.

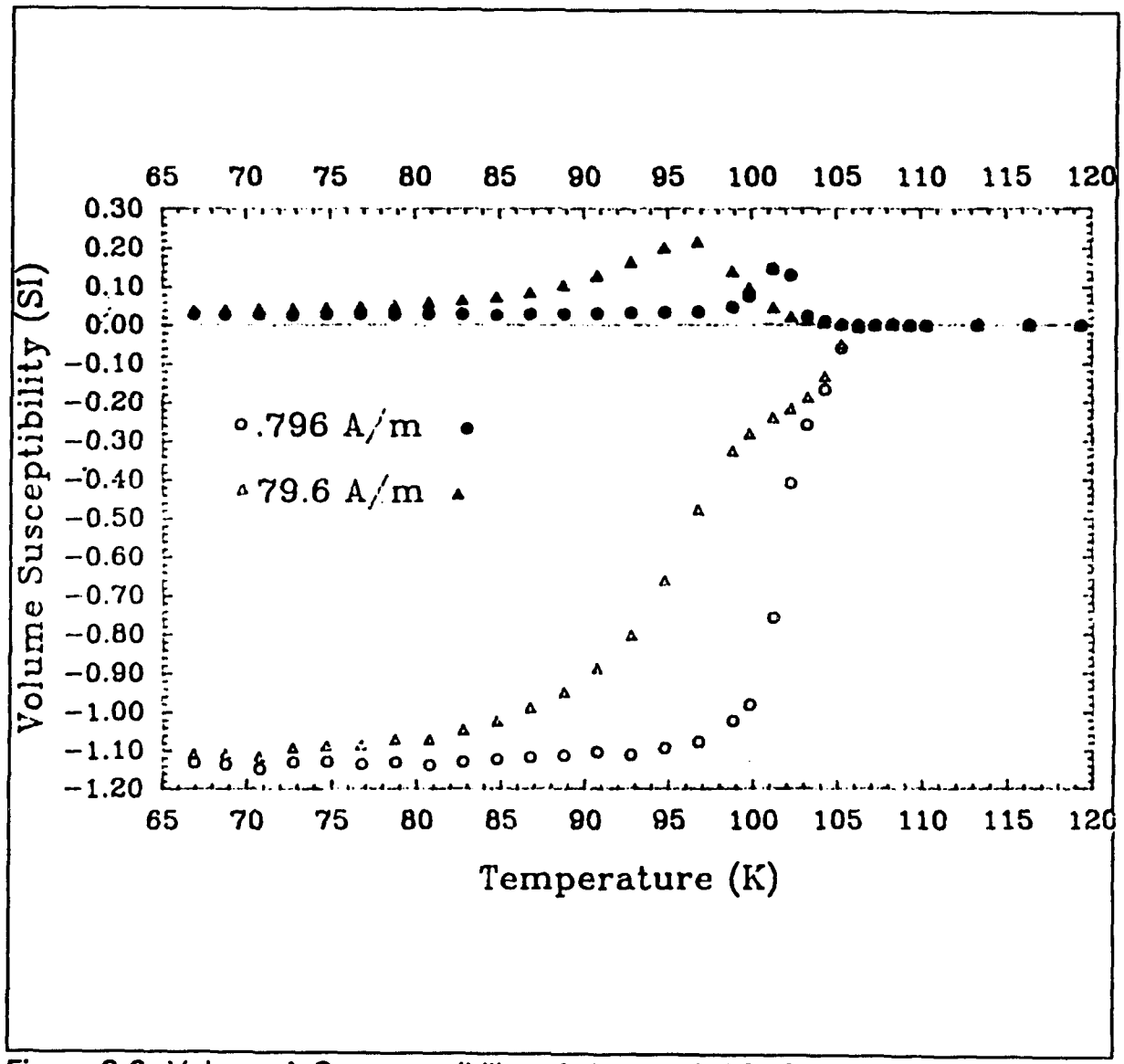

Figure 2.6 Volume A.C. susceptibility of sintered BiSCCO wire sample.

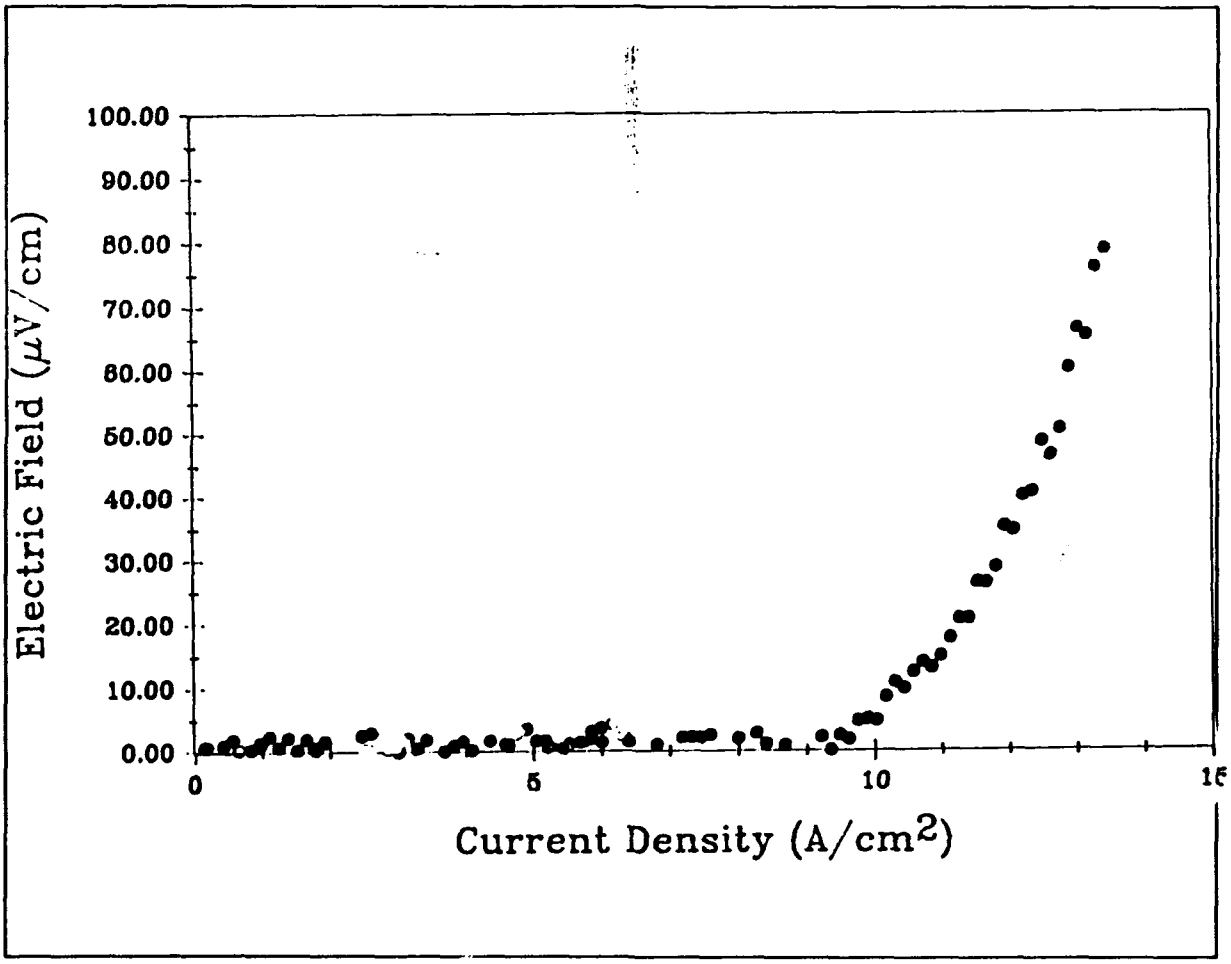

Figure 2.7 Current density versus field for a bare, sintered BiSCCO wire sample.

2.2. Fiber Spinning

Dana Eagles, George Bakis, and Wes Ishida
Albany International Research Corporation

2.2.1. Melt Spinning of Superconducting Ceramic Fibers

Fibers were spun from one batch of BPH5-2223 BiSCCO powder with diameters of 5 and 10 μm. The remainder of these green fibers are being stored under nitrogen for further use. No other fiber spinning operations were conducted during Quarter 10.

2.2.2. Winder Design

Work on the filament winder dedicated to the specific needs of green fiber spooling had been postponed during this quarter.

2.3. Wire and Part Development

David B. Chandler, Daniel Dexter, James D. Hodge, Matthew J. Neal, Mark V. Parish, Michael Parker, and Viren M. Pathare
CPS Superconductor Corporation

Continued wire development over this quarter has focussed primarily on the further enhancement of critical current densities. To this end, we have continued both our study of the continuous melt-texturing of $YBa_2Cu_3O_{7-\delta}$ fiber and wire and up until December 11, 1990, modification of our $YBa_2Cu_3O_{7-\delta}$ sintered wire process to produce mechanically textured BiSCCO ribbon. In addition, melt-texturing of bulk $YBa_2Cu_3O_{7-\delta}$ parts has received substantial attention to supplement the melt-textured fiber work as well as part of our efforts to produce a trapped flux motor. Each of these efforts are discussed below.

2.3.1. YBCO Sintered Wire

The $YBa_2Cu_3O_{7-\delta}$ sintered wire process has demonstrated that wire/fiber can be continuously produced in diameters ranging from 100 to 500 μm. The sintering facility presently in place can be used for continuous pilot-scale sintered wire production without major modifications. Accordingly, the continuous sintering process has not been developed further, but is routinely used to "presinter" the fibers used in the continuous melt-texture process.

In related work, as part of a Phase I SBIR program funded by the Army Center for Signal Warfare where CPS Superconductor and Foster-Miller Company, Waltham, MA are joint participants, we have extended our fiber technology to the production of wind-and-fire helical "coils" for use as high frequency (1 - 30 MHz) antenna components. Many shapes and pitches using varying fiber lengths and diameters were produced. Figure 2.8 shows several "coils" produced in this manner. Close-pitch, 1 cm diameter coils up to 21 cm long containing 8.5 m of 200 μm diameter sintered fiber have been produced. Self magnetic field critical currents at 77 K have been measured for each coil produced; typically, the J_c's of these sintered windings are in the 600-800 A/cm^2 range, with ~760 A/cm^2 measured through a 8.5 m sintered, coiled fiber sample. Coils such as these will be used to investigate the application of our melt-texturing techniques, helping to better define the melt-texturing process. Antenna related electro-magnetic results on measurements using these coils are presently being collected.

Figure 2.8 Several wind-and-fire type coils produced at CPS Superconductor as HF antenna components.

2.3.2. Melt-Textured $YBa_2Cu_3O_{7-\delta}$ Fibers

The CPS Superconductor fiber melt-texturing process, described in previous reports, involves a simple apparatus set-up where sintered fibers are slowly pulled through a small "micro-furnace" with a 25 mm long hot zone. Furnaces constructed this quarter use a temperature control system for improved process control, operating with a peak temperature of around 1100°C and a temperature gradient through the peritectic of at least 150°C/cm. During this quarter, we have explored the processing "envelope" for fiber melt-texturing, examining both fiber traverse rates and fiber diameter, as well as the feasibility of melt-texturing metallized fibers and post-melt-texturing metallized-coating possibilities.

Work has concentrated on defining the processing window to produce weak-link free, melt-textured $YBa_2Cu_3O_{7-\delta}$ filaments; the basic process was detailed in the 9th Quarterly Report. Immediate efforts are aimed at reproducible production of long lengths (up to 1 m) of high J_c, weak-link free fiber and defining the maximum processing rate. Processing parameters under investigation include: peak temperature, thermal gradient, fiber transit speed, and phase composition. The melt-texturing process is complex and sensitive, and this investigation requires a significant effort to achieve a stable and continuous manufacturable process. The manufacturable process requires engineering melt-texturing techniques. Equipment to supplement this effort will be investigated after achieving improved control and understanding of the basic process. To this end, three melt-texturing furnaces have been constructed, all similar, with only slight differences. Each furnace is made of

high resistance wire wrapped around a ceramic tube with added insulation. Temperatures in the furnaces are controlled to precise levels, adding to the overall control of the process.

In our melt-texturing process, the fiber is heated above the peritectic temperature decomposing the $YBa_2Cu_3O_{7-\delta}$ into Y_2BaCuO_5 plus a highly reactive liquid. The fiber's structural integrity is maintained due to the presence of surface tensions about an interlocking network of Y_2BaCuO_5 particles, thus requiring excess Y_2BaCuO_5. A supporting substrate cannot be used for melt-processing fiber because of the highly corrosive nature of the liquid phase, so a self-supporting fiber is pulled through the furnace. Experimental evidence suggests that 7.5 wt% Y_2BaCuO_5 additions are insufficient to maintain structural integrity of the fiber during this process while 22.5 wt% is adequate, though not necessarily optimum. Once decomposition has occurred and the molten portion has begun to cool through the peritectic, nucleation of the $YBa_2Cu_3O_{7-\delta}$ phase occurs. Initial observations suggest that the rate of nucleation and nature of the nucleation sites is likely to be consistent with classic nucleation and growth theory, though in our system the process is not yet well understood. Slow transit rates through the furnace result in the formation of a few large $YBa_2Cu_3O_{7-\delta}$ grains, with dimensions that approach the fiber diameter by a few centimeters in length. Higher transit rates result in a more polycrystalline microstructure, i.e., more numerous and smaller $YBa_2Cu_3O_{7-\delta}$ grains.

The electrical properties of the textured fiber seem largely determined by the apparent non-uniformity of the nucleation rate along the length of the fiber. This

non-uniformity has been identified in fibers processed at each of the two transit rates examined. The non-uniform microstructures may result from one or more of the following:

1) Fluctuations in the thermal gradient that cause local changes in the nucleation rate,

2) Segregation of impurities causes the crystallization front to be pinned, allowing new nucleation to occur in the supercooled region ahead of the pinned front, or

3) The transit rate through the furnace exceeds the crystal growth rate, increasing supercooling in the region ahead of the crystallization front, and thus increasing the local nucleation rate.

Microstructural examination of our melt-processed wire suggests segregation of the Y_2BaCuO_5 particles occurs only at higher transit rates. The non-uniform microstructures in these cases appear to be attributed to a combination of 2) and 3) above. At lower throughput, the microstructures suggest the condition described in 1). In any case, for a given transit rate through the furnace and fiber composition, a unique set of values of peak temperature, thermal gradient at the peritectic, and fiber supercooling should exist where a stable crystallization front can propagate. These parameters are being determined as they constitute a mandatory requisite to develop a manufacturable process.

A major priority this quarter has been correlating optical microstructures with electrical properties. To date, the highest J_c values ($>20{,}000$ A/cm^2 in self magnetic field) are obtained for samples containing a minimal number of grains (i.e., a few large grains). However, respectable J_c values ($>5{,}000$ A/cm^2 in self field) have been obtained on the more polycrystalline, smaller grain size samples produced at higher

transit rates. This performance in more polycrystalline samples may be due to a higher probability of the existence of pathways along the fiber through well aligned or low angle grain boundaries that do not exhibit weak-linked behavior. Several 90^{+} cm long melt-textured fibers were processed at the higher transit rate. So far, one of the fibers tested carried an impressive 5 A through the entire length in a 1 T applied magnetic flux density.

Metal cladding is an important and integral part of our program. There are mechanical, environmental, and electrical advantages of our metallic coating. Earlier in our program, we developed a process where green fiber was coated with a slurry containing metal followed by a continuous cofiring process. Preliminary attempts of melt-processing silver and silver-palladium pre-cofired filaments resulted in mixed success. Silver-palladium coated filaments display the melt-textured microstructures similar to bare filament melt-processed samples, but have a palladium-contaminated region at the ceramic-metal interface. This interfacial region is believed to reduce the electrical performance of the melt-texture fibers, resulting in critical current levels about 40% lower than similarly processed bare fibers. Though there are plans for more tests and experiments in the area of melt-texturing metal coated fibers, more promising and more immediately available work has progressed in the area of post-melt-process coating. In this procedure, the melt-processed bare fiber is coated with a silver slurry and post-fired at a temperature quite a bit lower than the melt-processing temperatures, though adequately high enough to sinter the silver to the fiber-substrate. This method of post-process coating the fiber produces a very good

electrical contact of metal-to-ceramic superconductor and has not degraded the electrical performance of the melt-processed fiber, though the oxygen anneal time must be extended.

2.3.3. Melt-Textured $YBa_2Cu_3O_{7-\delta}$ Disks

Preparation of melt-textured disks, aimed primarily at the fabrication of components for the Emerson Motor Division-designed "trapped flux" motor, complements our melt-texturing fiber work since it allows a quicker examination of the melt-texturing process under radically different conditions of temperature and thermal gradient. The preparation of melt-textured disks and rings complement each other as well. The rings are planned to be cut from disks, thus the disk work will naturally precede the ring effort. The requirements of producing disks to test the motor design are much less demanding than those of the rings, so that the time from initiating an experiment until testing the disks in the motor is shorter. However, as is explained in detail in Section 2.4. below, the electrical, magnetic, and mechanical demands on the pellets are much higher than on the rings while in the operating motor. The disk-design relies on circulating currents in the grains of the disks, the ring-design relies on circulating current through the ring itself--a more difficult situation. Our initial calculations show that the current in the rings (that trap magnetic flux in the steel rotor poles they surround) can be more than an order of magnitude less than that required in each grain of the disks (that traps magnetic flux in the disk as a whole) to produce a motor of comparable performance. Additionally, the iron poles in the ring-design motor accept the bulk of the mechanical stress while

the motor is in use, whereas less favorably, the actual ceramic in the disk-design motor supports much of the stress. Clearly, the ring motor design will be the ultimate goal of this portion of the work, but the disks allow more immediate testing of the motor.

The initial production of melt-textured disks had been limited by the existence of a centralized "core" of untextured, polycrystalline $YBa_2Cu_3O_{7-\delta}$ as was reported in the last quarterly report. The inverse linear dependence of the core volume on time and temperature above the peritectic indicates slow heat transfer into the disk interior. In addition, since a 25 gram disk requires more than 36 minutes to reach thermal equilibrium above the peritectic, the peritectic reaction must be highly endothermic in nature. With this understanding, we currently produce core-free melt-textured disks. The grains appear to be not fully aligned, which is acceptable to trap magnetic flux since the induced currents need only be circulating within each grain. Now that the disks are being produced with uniform microstructures, attempts to optimize the microstructure, that is, maximize the grain size, will be tested to maximize the circulating currents in each grain.

The melt-processed rings, on the other hand, require a great degree of grain alignment or low angle grain boundaries. The weak-links must be minimized, or ideally, eliminated (i.e., single grain), so that an induced current is allowed to circulate through the ring as a whole. Development techniques that have been initiated to address grain alignment show promise.

It has been demonstrated that the recrystallization of $YBa_2Cu_3O_{7-\delta}$ is extremely sensitive to the presence of even small thermal gradients. Disk samples melt-processed in $MoSi_2$ box furnaces clearly show evidence of $YBa_2Cu_3O_{7-\delta}$ nucleation at surfaces not directly exposed to the heating elements, i.e., the cooler surfaces of the sample, and subsequent growth toward the hotter regions. This preferential nucleation and growth of $YBa_2Cu_3O_{7-\delta}$ has served to illustrate the tendency of Y_2BaCuO_5 particles to be pushed ahead of the growing crystallization front--even in samples with no added Y_2BaCuO_5. The result of accumulating Y_2BaCuO_5 particles ahead of the growth is the "pinning" of the crystallization front. Secondary crystallization then occurs in the Y_2BaCuO_5-rich region ahead of the front forming spherulitic crystals of $YBa_2Cu_3O_{7-\delta}$. The nucleation of these spherulites appears to be random with the growth occurring until impingement upon their neighbors.

The preferential nucleation and growth of $YBa_2Cu_3O_{7-\delta}$ in very small thermal gradients may allow grain alignment to be induced while processing the rings. Since the (103) pole is the direction of fastest growth, a thermal gradient perpendicular to the disk axis should cause a high degree of grain alignment during melt-processing. We intend to induce a thermal gradient by cooling the top of a disk with a gentle flow of air as the temperature is lowered through the peritectic. Initial tests have been unsuccessful; improved control of the air flow and thermal scheduling should serve to improve the process.

The segregation of Y_2BaCuO_5 particles ahead of the crystallization front, evident in melt-textured disks but not fibers, appears to be due to the difference in the thermal gradient at the peritectic. When the thermal gradient is large, as for fibers, the driving force for crystallization is sufficient to sweep past and trap Y_2BaCuO_5 particles. When the thermal gradient is small as in the disk processing, the crystallization driving force is proportionally reduced and Y_2BaCuO_5 particles become segregated ahead of the growth front. This segregation of Y_2BaCuO_5 presents a problem in melt-processing large samples since the melt-texturing dimension is effectively limited to about 5-7 mm (by observation). However, this issue might be avoided with the use of heat baffles to produce a more truly isothermal environment. In an isothermal environment, nucleation and growth obeys the classic theory and occurs randomly allowing the entire sample to be melt-textured. The isothermal environment is currently being improved for the processing of the disks. In addition, the thermal gradient will be improved for both the fiber processing (by designing a new furnace), and for the ring/disk processing by incorporating a directional heat source or heat sink.

2.3.4. BiSCCO Wire Development

An effort has been carried over from the past quarter involving the adaptation of the CPS Superconductor sintered wire process to the production of textured BiSCCO ribbon wire. Briefly, our concept is to produce silver-coated green BiSCCO-2223 fiber, sinter this fiber at a temperature high enough to densify the Ag coating,

mechanically roll the wire into a thin ribbon to induce orientation in the BiSCCO, and subsequently anneal this ribbon to optimize the material's superconducting properties.

The initial process work described here was performed on non-optimized powder to allow us to evaluate both continuous sintering and rolling. The ribbons produced from this powder were subjected to post-rolling anneals for 48 hours at temperatures between 830 and 850°C in air. All of these samples showed evidence of necessary liquid phase formation, but also excessive degradation. Fibers have been made with optimized powder to be used to produce similar ribbons for experiments aimed at optimizing the post-fire annealing process. See the discussion of preliminary results in Section 2.1.2. As previously mentioned, the BiSCCO work was terminated for the remainder of this program.

2.4. Motor Design and Fabrication

Alan Crapo and Jerry Lloyd
Emerson Motor Company
Mohamed Hilal
University of Wisconsin

The Emerson Motor Division (EMD) of Emerson Electric Company has designed, built, and tested motors to be used with HTSC materials. In designing and building HTSC motors, two major objectives were addressed: The first, develop a motor to test HTSC wire produced by CPS Superconductor, and the second, to design and build a motor that takes advantage of the characteristics of the presently-developed, newly developed HTSC materials. The homopolar DC motor that had been designed,

built and tested (with copper windings) for HTSC wire is ready when long lengths of weak-link free conductors are available. The second design, described in the last quarterly report, uses melt textured disks and rings. Further development on this motor is described below.

Bulk HTSC materials were tested for magnetic flux trapping capability and the ability of the superconductor to circulate persistent currents to trap magnetic flux in an iron rod. The test results are presented and discussed. The previously presented trapped magnetic flux motor design is shown for versions using HTSC rings around the rotor poles and HTSC disks at the end of the poles. Initial test results and analytical data of the two motor's performances are presented.

2.4.1. Trapped Magnetic Flux Measurements.

An attempt was made to measure the magnetic flux trapped in an iron magnetic circuit due to persistent transport current around HTSC rings. Even though the rings seemed to have good Meissner properties indicating good J_c within grains, the persistent transport current in the ring was too low to measure. The grain boundaries apparently create weak links or barriers to transport and do not allow the current circulate freely through the ring.

A small block shaped sample of bulk melt textured Y-123/15% Y-211 with dimensions of 1.0 cm X 0.9 cm X 0.65 cm was one of the first samples supplied for testing. Using a copper wound C-core magnetic circuit, a magnetic field was applied to the HTSC block while in its normal state. The magnetic field was measured with a search coil and integrating magnetic fluxmeter. The plot of the

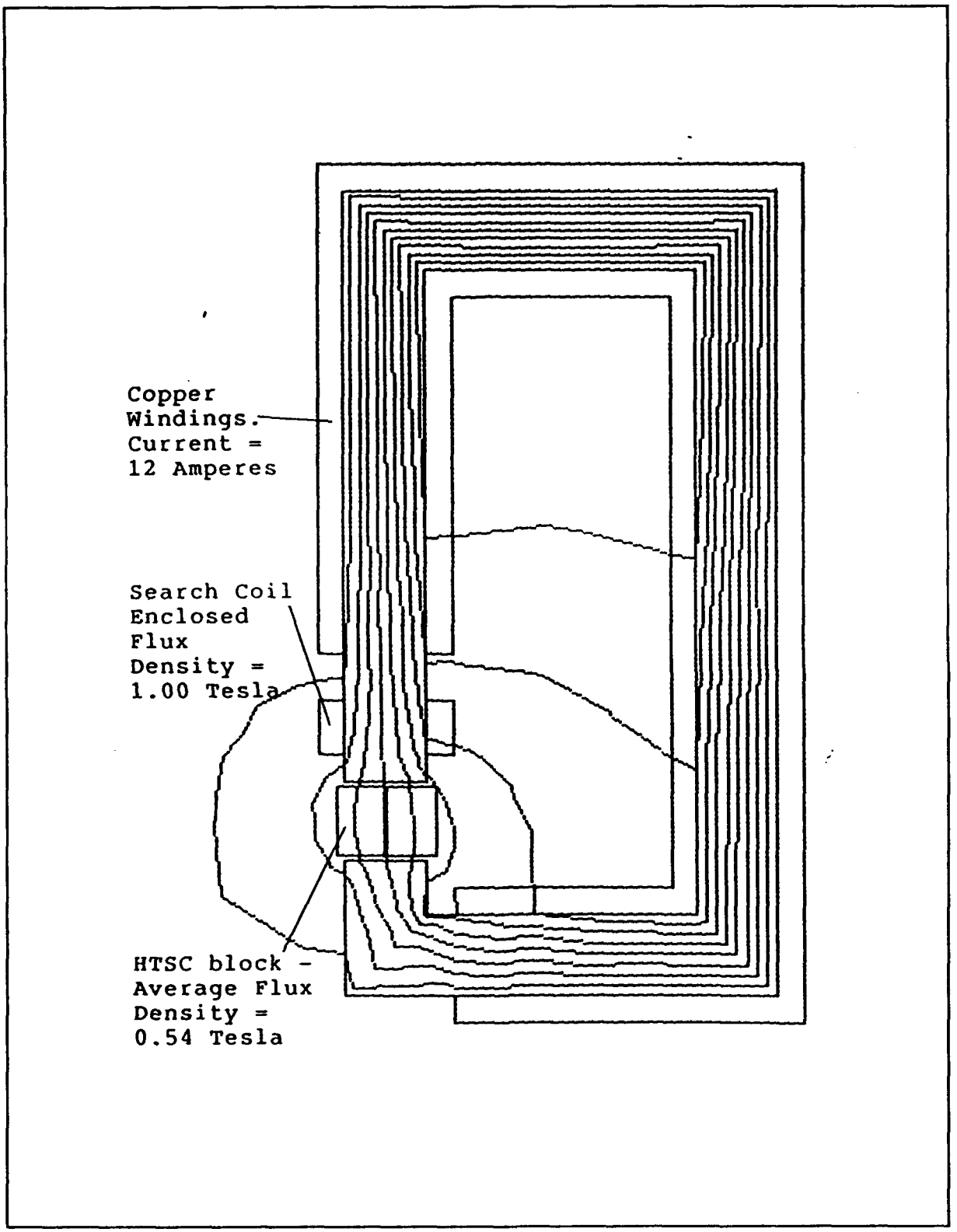

Figure 2.9 Magnetic field applied to HTSC block by C-core.

finite element model in Figure 2.9 shows the magnetic field applied to the HTSC block by the C-core magnetic circuit. The ratio of magnetic flux density at the HTSC block to the magnetic flux density at the measurement coil is about 54%.

The melt-textured sample block was cooled with liquid nitrogen while the applied magnetic field was maintained. After the sample was cooled to 77 K, the applied magnetic field was removed. Induced currents within the sample maintained a magnetic field within the block. Figure 2.10 shows the finite element model based on uniform current distribution within the sample block. The block was then removed from the magnetic circuit and the change in the indicated magnetic flux at the search coil was recorded. This change in the measured magnetic flux is equal to that trapped in the block while in the magnetic circuit. In this case, the magnetic flux at the HTSC block is 106% of the magnetic flux through the search coil.

Figure 2.11 shows the magnetic flux trapped in the sample block with no magnetic circuit. With the magnetic circuit removed, higher current density is required to keep the same magnetic flux trapped. The trapped 350 Gauss in the tested sample corresponds to a uniform intragranular current densities of 2388 A/cm^2. When the block was once again placed into the magnetic circuit, the magnetic flux that remained trapped was measured. Figure 2.12 shows the trapped magnetic flux density versus the applied magnetic flux density. The upper curve shows the initial magnetic flux trapped in the HTSC block, and the lower curve shows the magnetic flux trapped in the sample block after the block had been removed and then returned into the magnetic circuit. It seems that the 2388 A/cm^2 that corresponds to

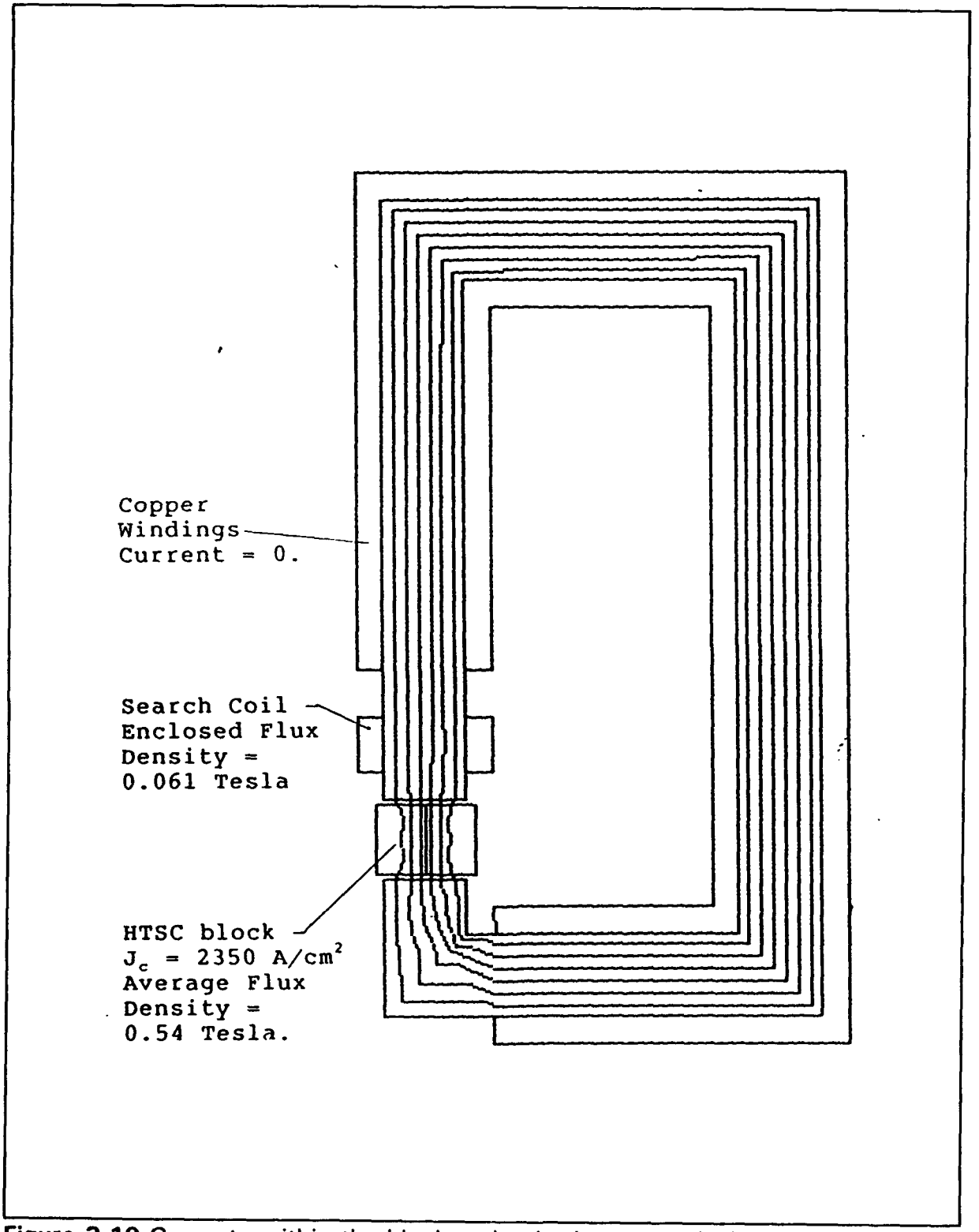

Figure 2.10 Currents within the block maintain the magnetic flux.

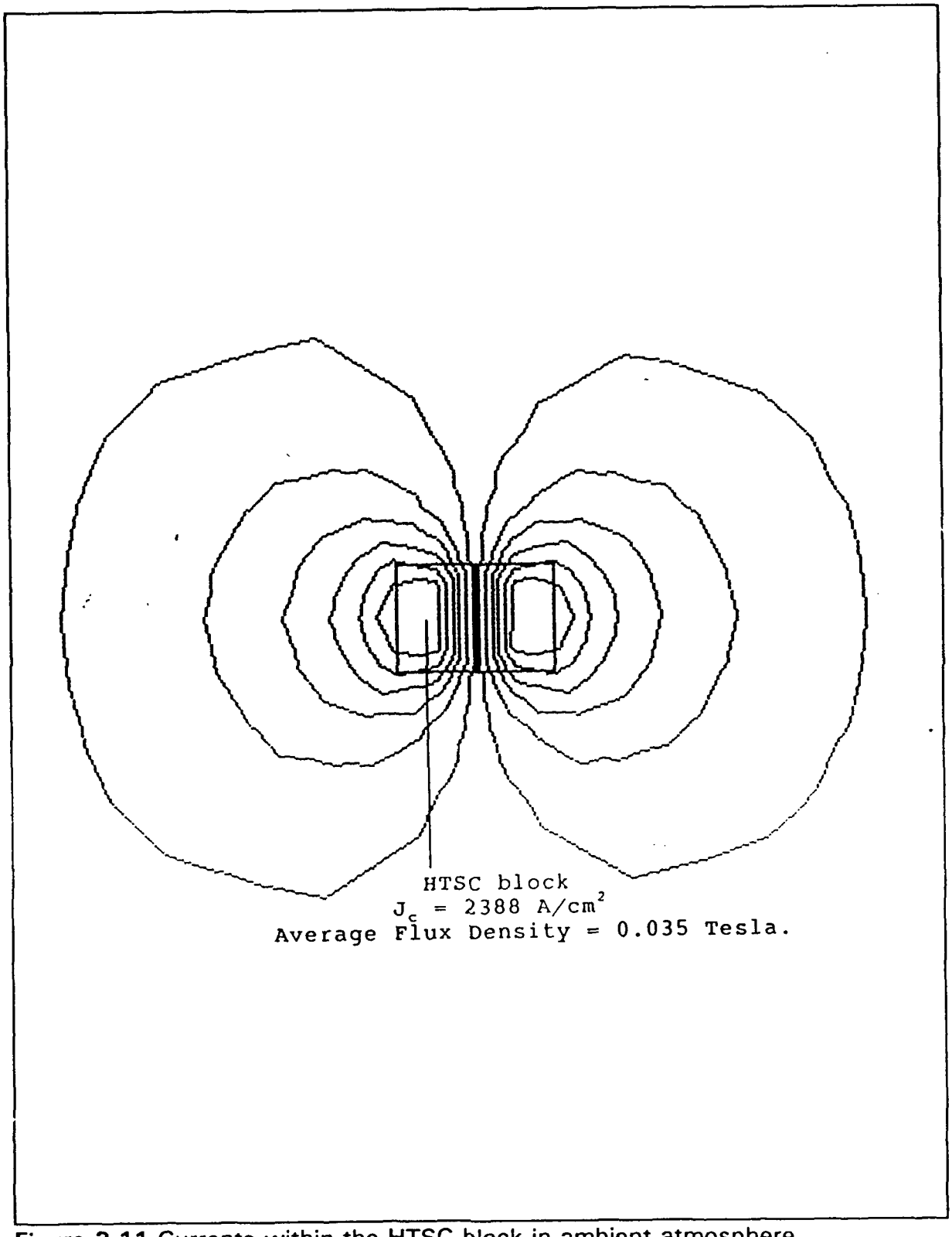

Figure 2.11 Currents within the HTSC block in ambient atmosphere.

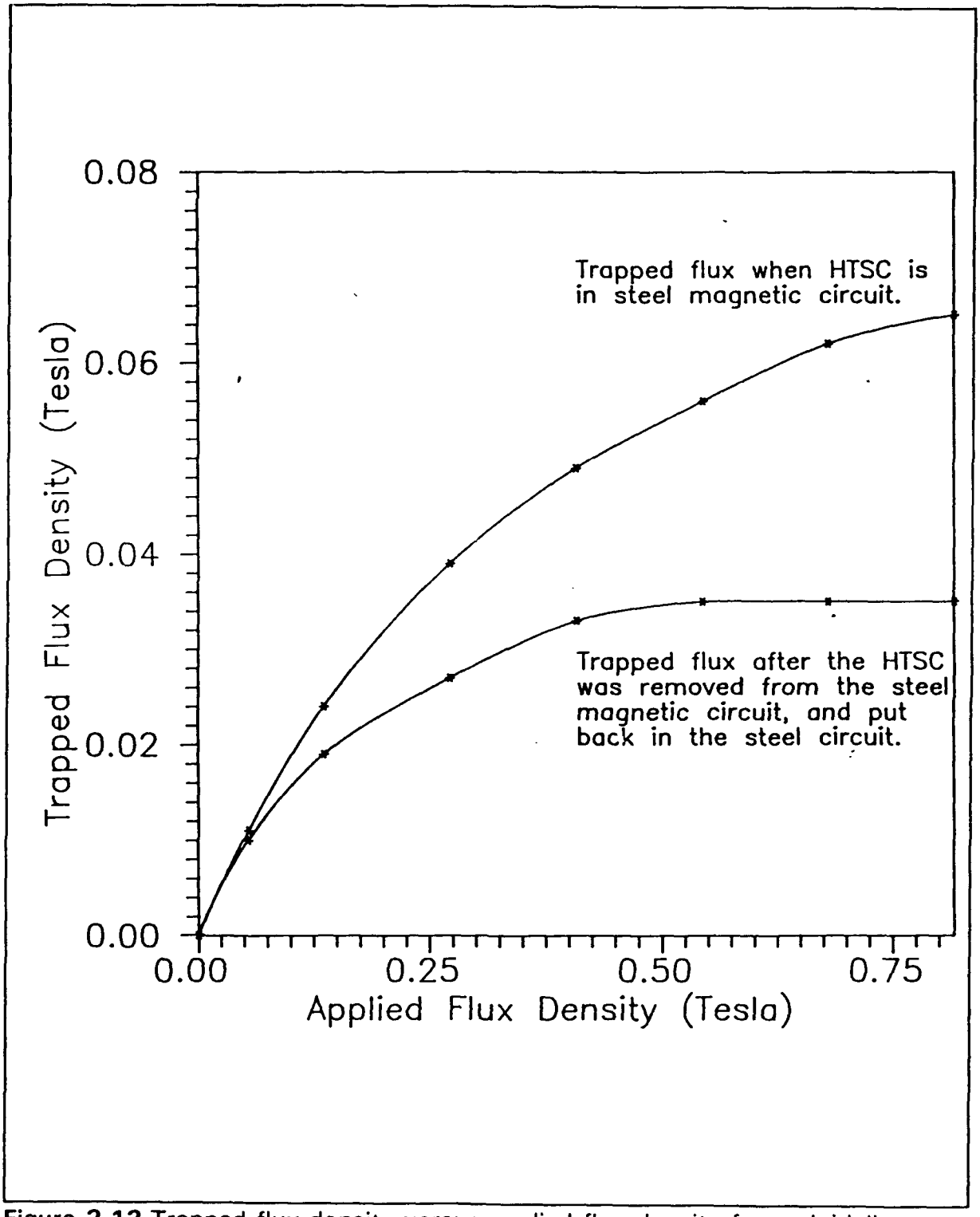

Figure 2.12 Trapped flux density versus applied flux density for an initially warm HTSC block.

350 Gauss of trapped magnetic field is about the maximum effective average J_c for the block under these conditions.

The most effective way to trap magnetic flux in HTSC disks is to apply the magnetizing field while the HTSC temperature is above T_c and then cool to below T_c. An attempt was made to trap magnetic flux by forcing the magnetic flux into the superconductor after it was cold since this represents a convenience in HTSC motor applications. If the magnetic field is high enough, the limited effective J_c will not completely exclude the magnetic flux. When the applied magnetic field is removed, some magnetic flux should be trapped. Figure 2.13 shows the trapped magnetic flux density versus applied magnetic flux density for the cases of the HTSC starting out above T_c (warm) and below T_c (cold). Figure 2.14 shows the difference in trapped magnetic flux when the HTSC block is removed from the magnetic circuit, and then put back into the c-core. Both curves are for the HTSC block starting out below T_c.

2.4.2 Brushless DC "Trapped Flux" HTSC Motor

A brushless DC trapped magnetic flux motor that had been designed and built was presented in Quarterly Report 9 for bulk HTSC rings; the rotor and stator of this motor are shown in Figures 2.15 and 2.16. As originally designed, the magnetic flux is trapped in the steel by transport persistent current in the rings. Due to the permeability difference between the steel and the superconductor, the magnetic flux density at the superconductor is advantageously much lower than it is in the steel pole. In order to produce a successful motor, the rings must have good transport J_c through the entire loop. As mentioned above, initial samples tested did not support

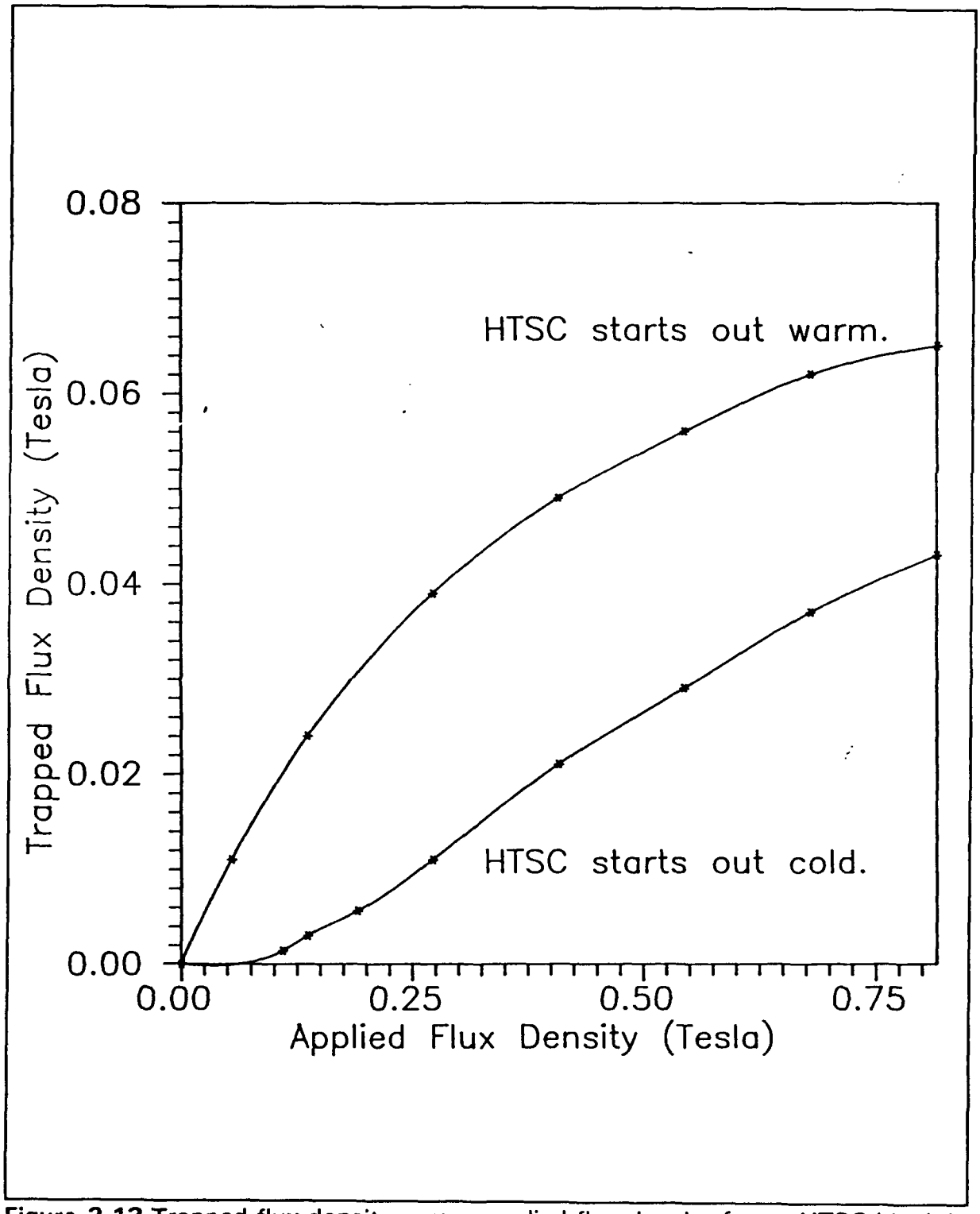

Figure 2.13 Trapped flux density versus applied flux density for an HTSC block in a steel magnetic circuit.

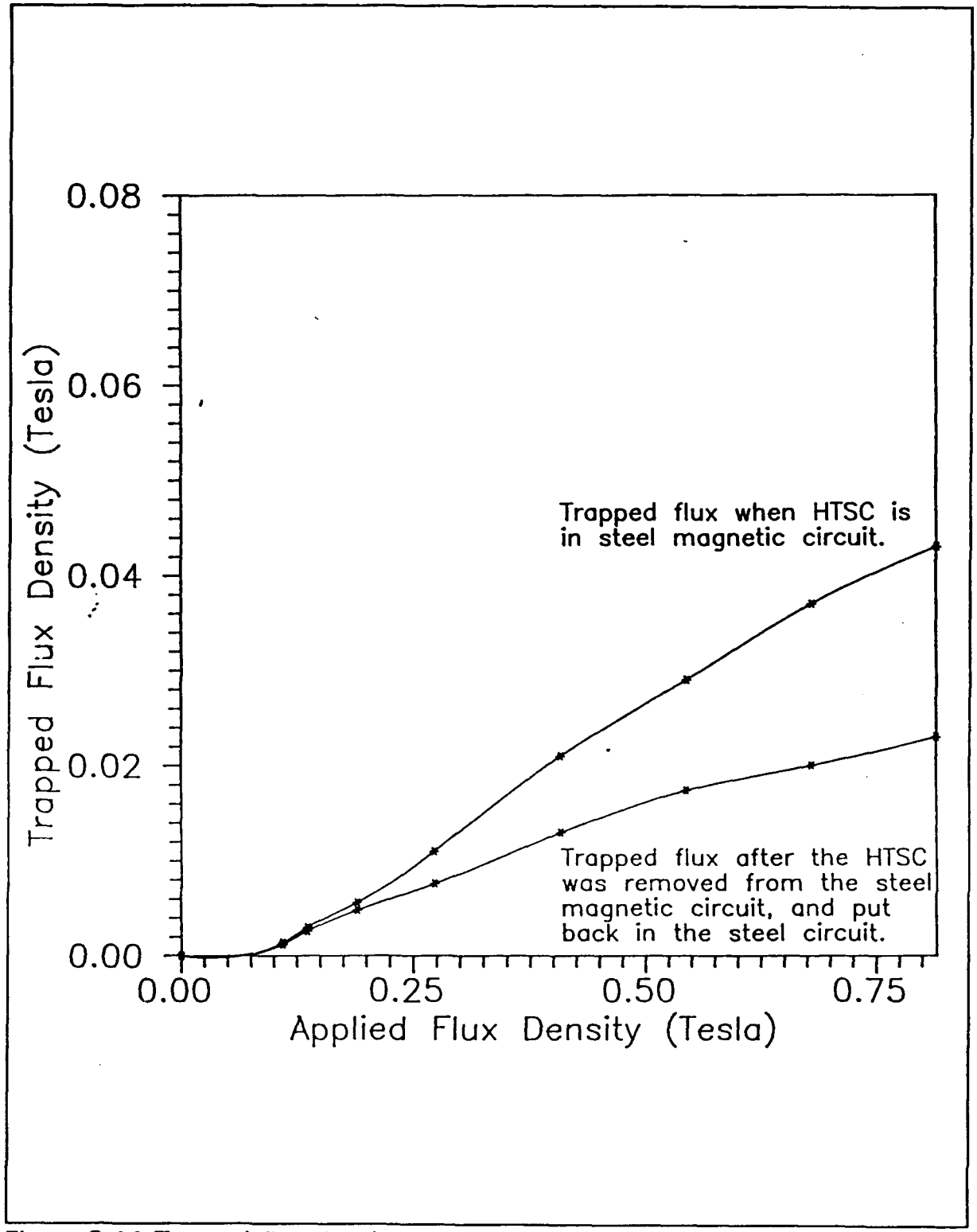

Figure 2.14 Trapped flux density versus applied flux density for an initially cold HTSC block.

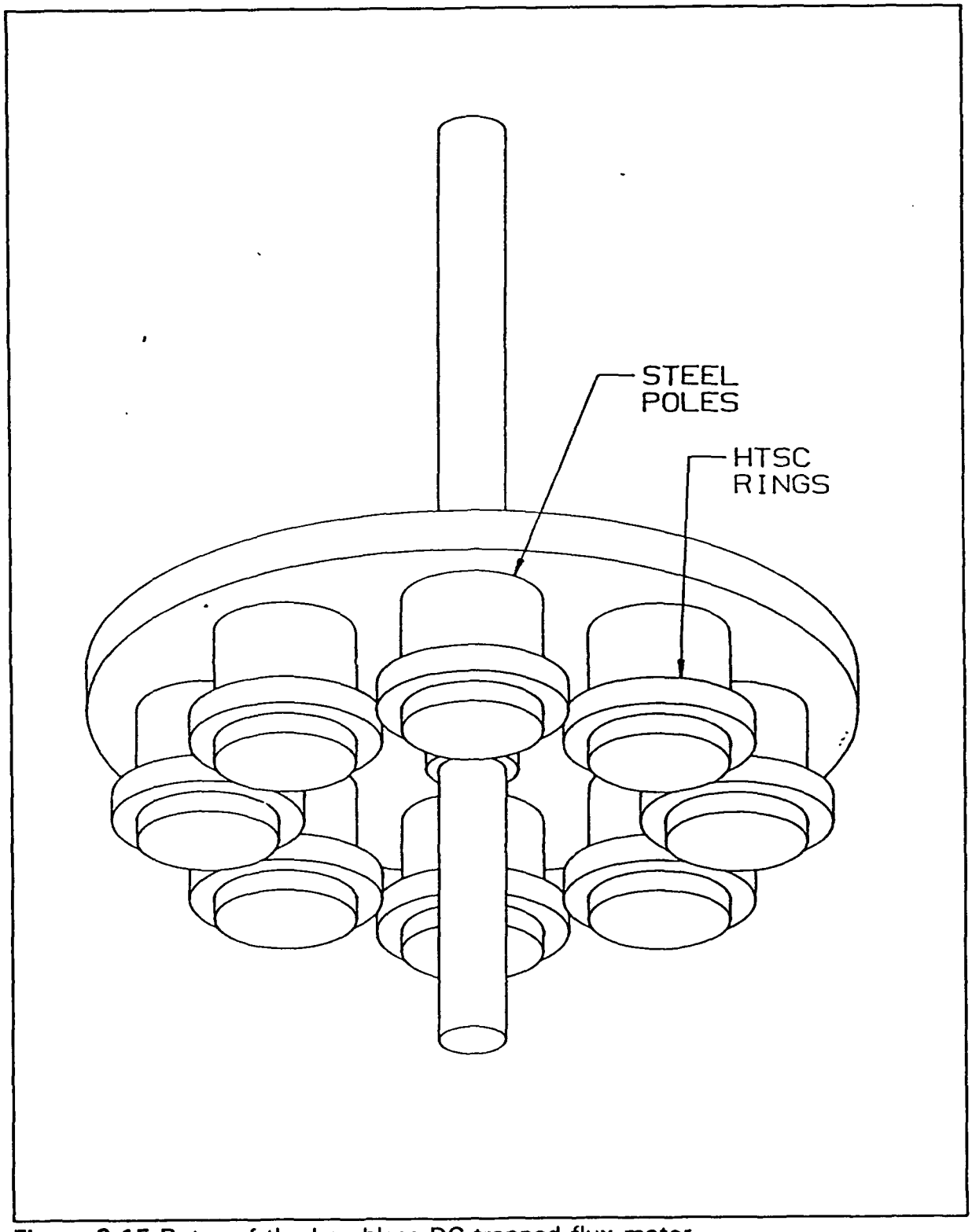

Figure 2.15 Rotor of the brushless DC trapped flux motor.

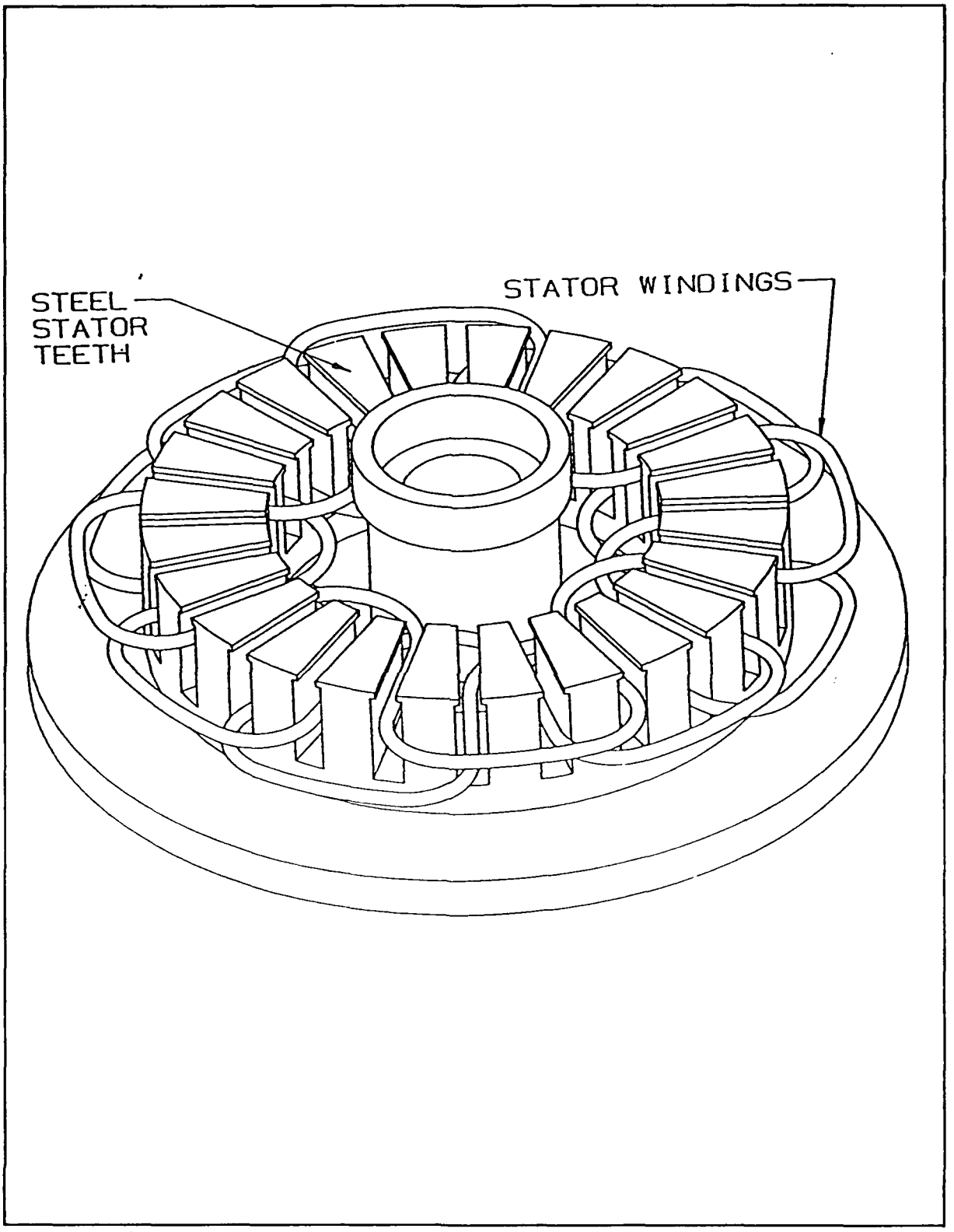

Figure 2.16 Stator of the brushless DC trapped flux motor.

significant transport current in the rings, leading to a modified motor design.

Early attempts to trap magnetic flux in disks or blocks of HTSC material had resulted in 300 Gauss retained, so efforts were made to improve that mark and modify the motor to work with disks at the end of each of the eight poles instead of rings about the poles. The next step was to model the ring version and the disk version of the motor with the same constant parameters for comparative purposes.

To compare the two motor designs, finite element modeling was used to calculate the applied magnetic field produced by the stator and the magnetic field that can be trapped by circulating currents in the two designs. With the disks placed in the air gap at the ends of the steel poles, more current is needed in the stator to produce an applied magnetic field at the superconductor than for the ring version.[3] Figure 2.17 shows curves of the measured applied magnetic field at the rotor pole versus stator current for the ring and disk versions of the motor. Since the ring version has a much smaller non-iron (air) gap, it takes less current to maintain magnetic fields in the rotor than the disk version. Figure 2.18 shows the magnetic flux plot of the brushless DC motor with an HTSC ring with 800 A (1240 A/cm^2) of persistent current trapping 1.01 T magnetic flux density in the rotor pole. Figure 2.19 shows a magnetic flux plot of the motor with an HTSC disk with 8000 A trapping an average of 0.81 T in the disk and the rotor. Assuming that the disk is one large grain and that the current is uniformly distributed, 8000 A corresponds to 12,400 A/cm^2.

[3] The effective air gap distance between the base of the steel pole and the stator windings is increased by the thickness of the HTSC disks.

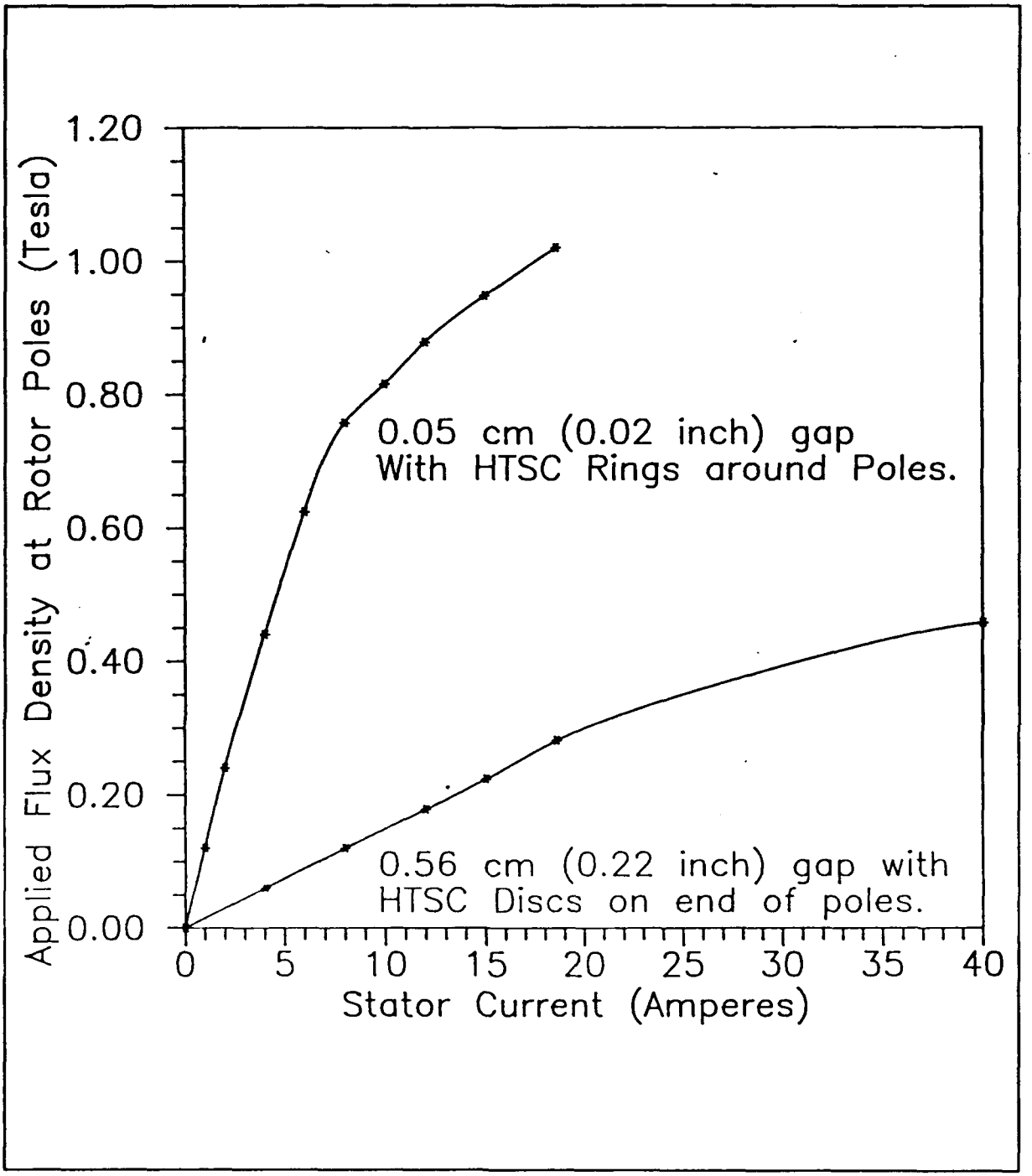

Figure 2.17 Measured flux density at the rotor poles versus the current in the stator.

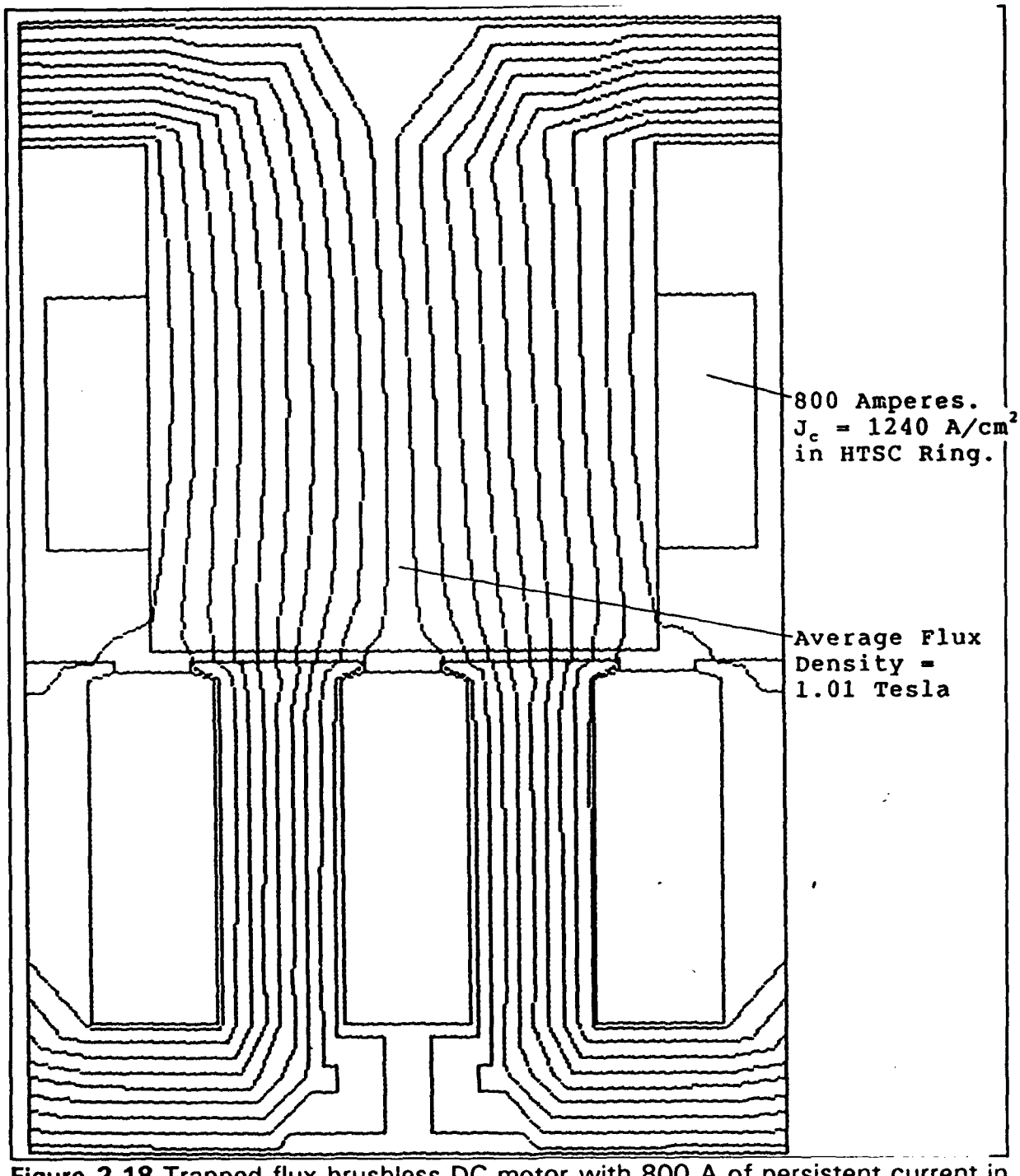

Figure 2.18 Trapped flux brushless DC motor with 800 A of persistent current in an HTSC ring.

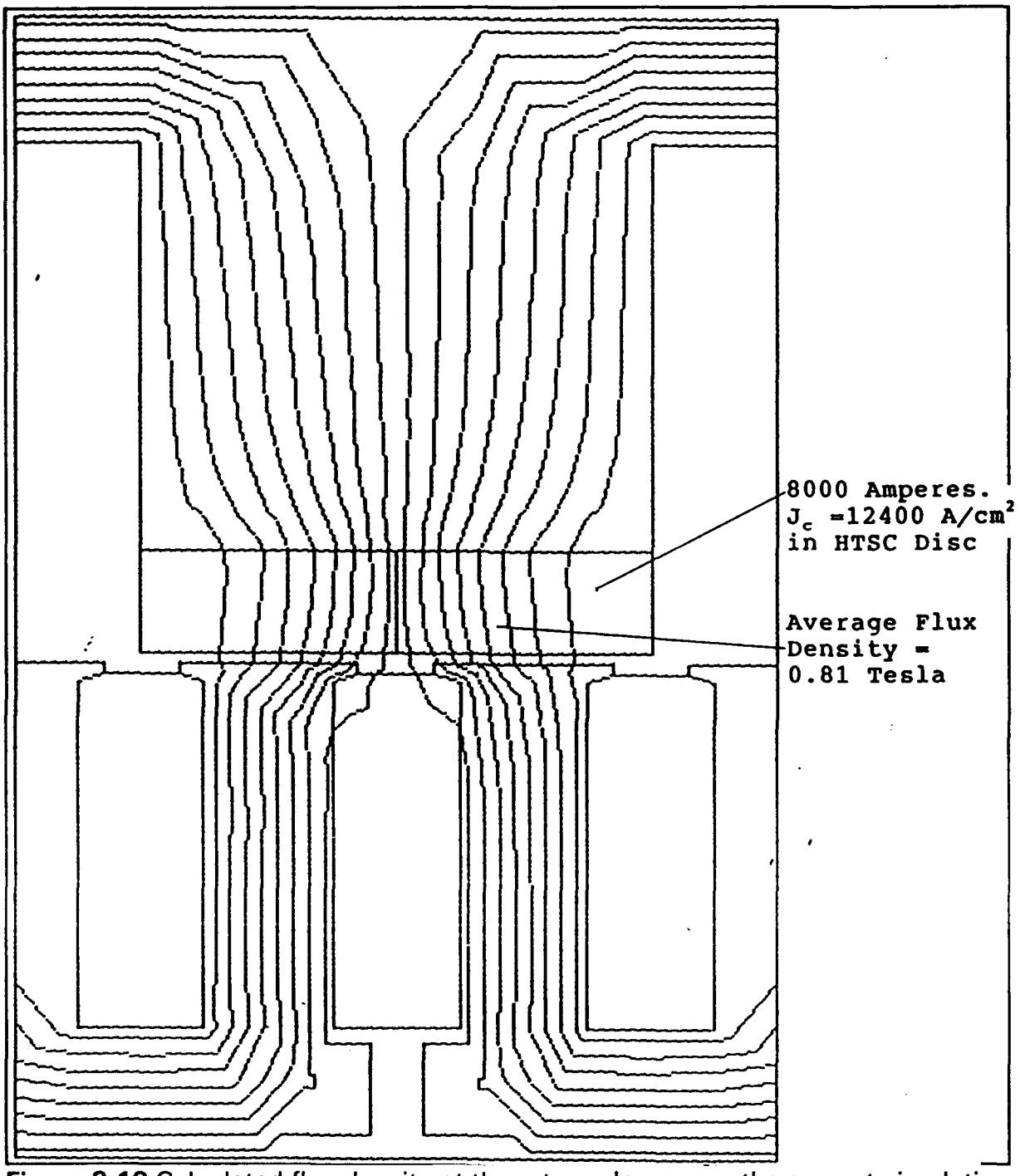

Figure 2.19 Calculated flux density at the rotor poles versus the current circulating in the superconductor.

If the disk is made up of several smaller uniform grains, then each grain must have 8000 A circulating current with much higher individual current densities.

Figure 2.20 shows plots of trapped magnetic flux density at the rotor poles for ring and disk superconductors for several values of current in the superconductors based on a uniform current distribution in a single grain. Since the purpose of trapping magnetic flux is to produce magnet replicas, ferrite and rare earth permanent magnet trapped magnetic flux levels are shown. The ring superconductor takes 200 A to trap magnetic flux comparable to a ferrite magnet, and 800 A to trap magnetic flux comparable to a rare earth magnet. The disk superconductor takes 4700 A (23.5 times the ring version) to trap magnetic flux comparable to a ferrite magnet and 10600 A (13.25 times the ring version) to trap magnetic flux comparable to a rare earth magnet. The cost of ferrite magnet material is about $4.00 per kilogram and the cost of rare earth magnet material is about $130 per kilogram.

Combining the data from the tests of measured magnetic field versus stator current and the trapped magnetic field versus applied magnetic field, the trapped magnetic flux of an HTSC motor versus stator current can be estimated. Figure 2.21 shows this curve. A trapped magnetic field of 0.05 T should be attainable. Correspondingly, four amperes in the stator produces a stator magnetic field of about 0.05 T. A trapped magnetic flux motor with 4 A of current should produce 0.28 N-m of torque. Although this is an order of magnitude lower than the motor was originally designed, it will still produce enough torque to spin the motor--more than

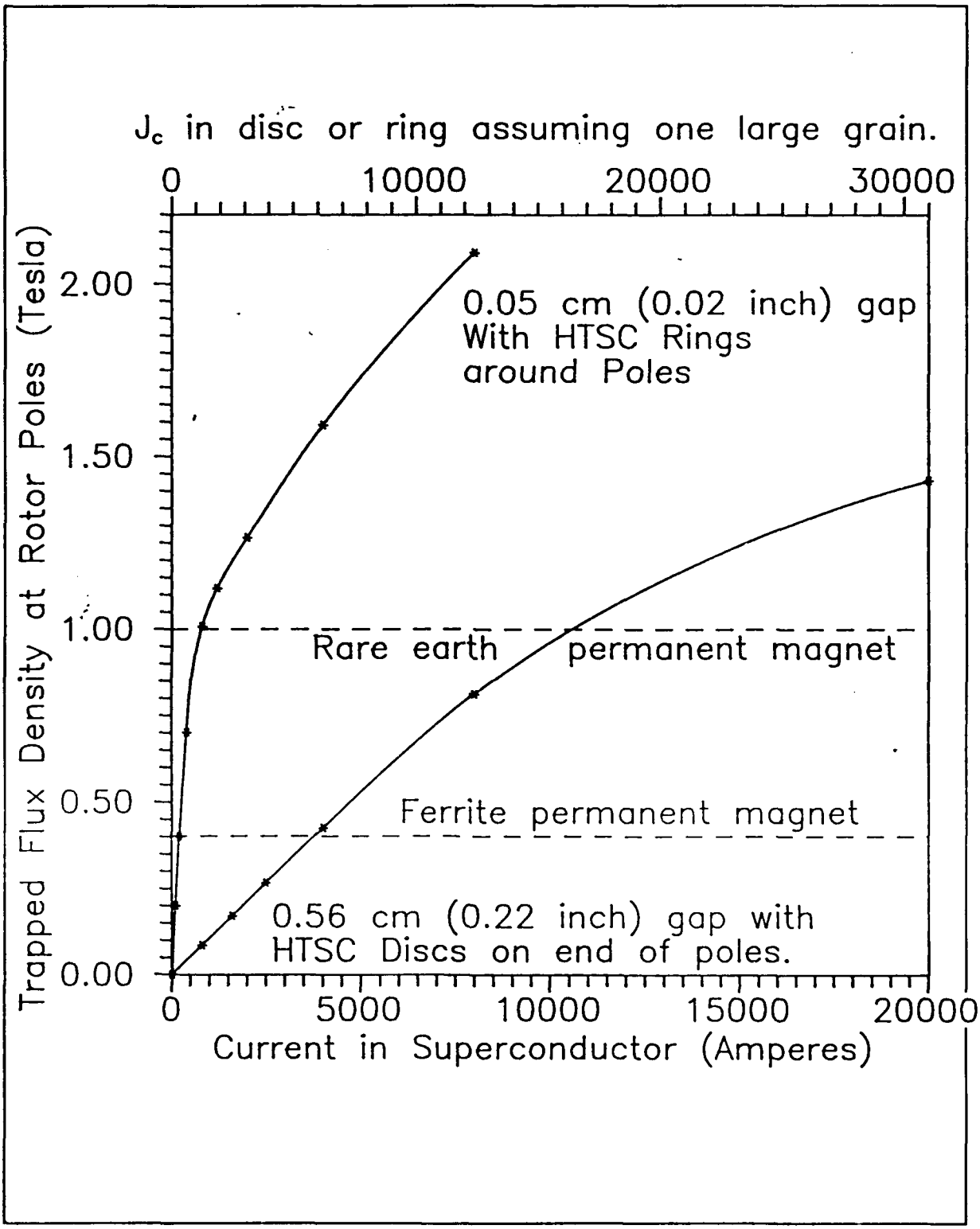

Figure 2.20 Calculated flux density at the rotor poles versus the current circulating in the superconductor.

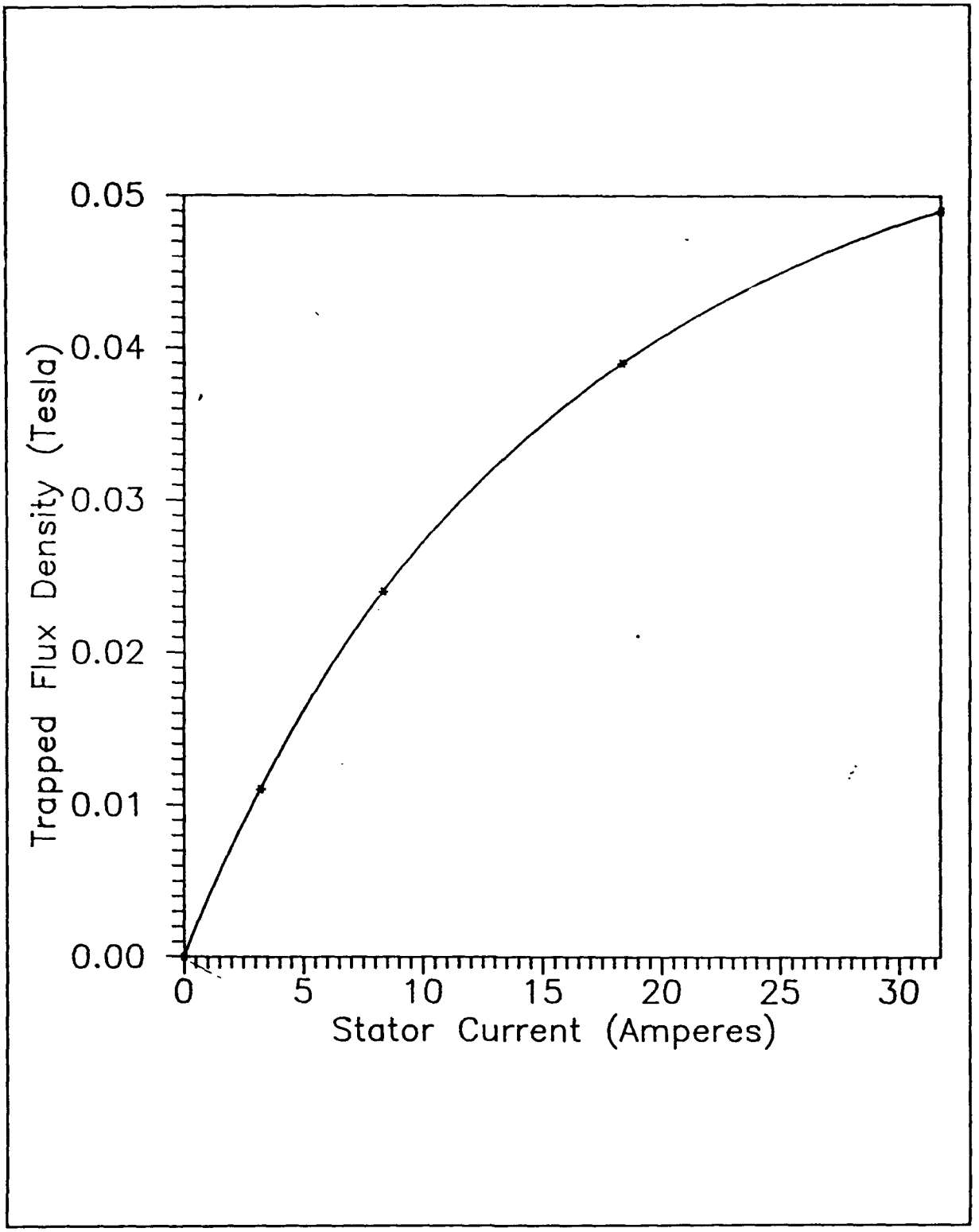

Figure 2.21 Trapped flux density versus stator current for HTSC discs in the air gap at the end of the poles.

20 times greater than the bearing friction--demonstrating the feasibility of using bulk HTSC in and electrical motor.

Until the characteristics of applied magnetic flux versus trapped magnetic flux for the HTSC ring around a steel pole are better understood, it is difficult to calculate motor performance with HTSC rings. Ignoring how much applied magnetic field it takes to trap magnetic flux with persistent transport current around a ring, and assuming that the stator magnetic field under load should not exceed one half of the trapped magnetic field, the torque capability of the motor for various values of J_c in the rings can be calculated as plotted in Figure 2.22. Magnetic flux saturation of the steel poles distortion is evident in the shape of the curve.

As the melt-textured ring work progresses and a number of reproducible samples are constructed, testing on the motor will proceed.

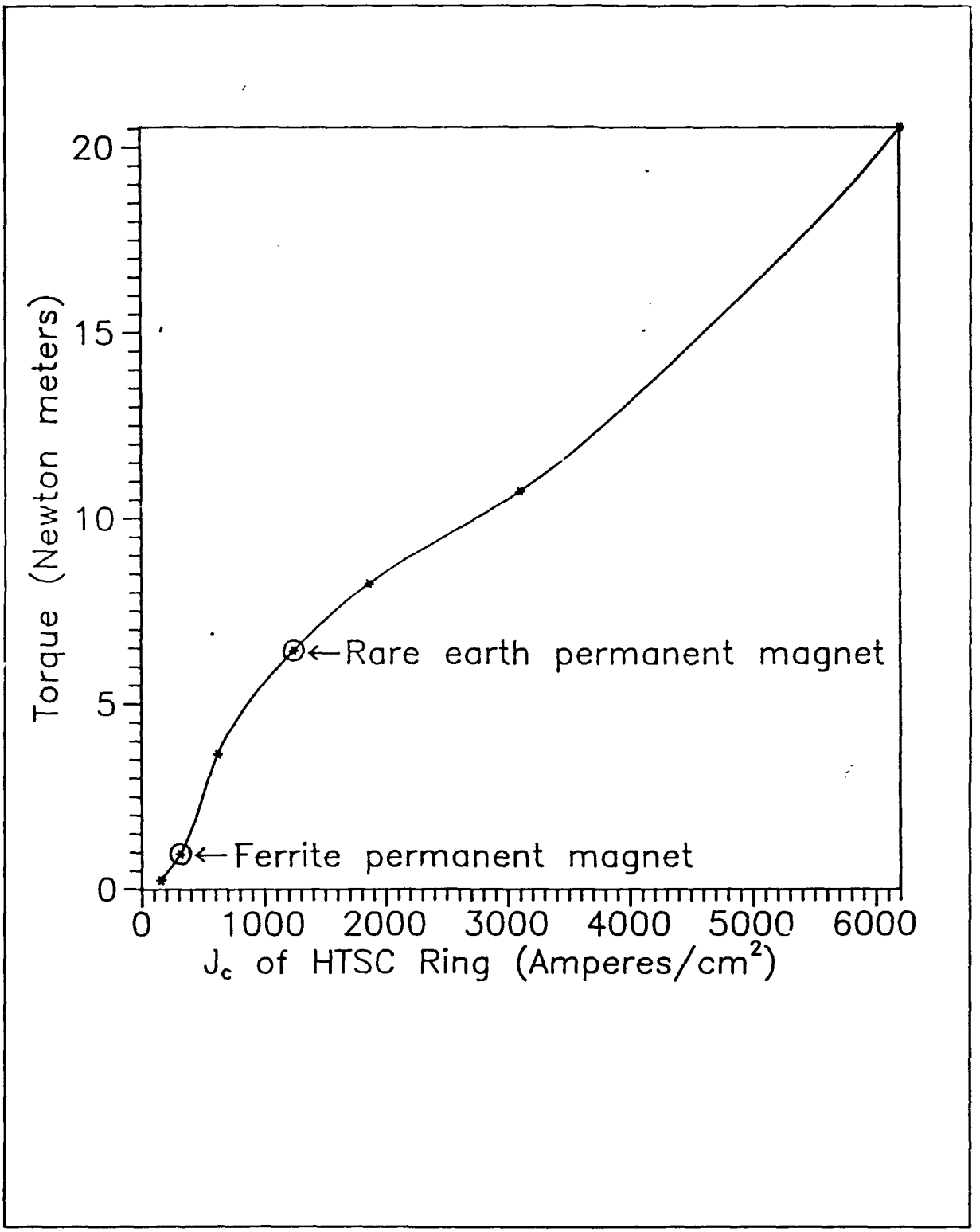

Figure 2.22 Theoretical torque capability of the ring version of the trapped flux motor versus J_c in the HTSC ring.

3. GOALS FOR FUTURE REPORTING PERIODS

The coming quarter will see a continuation of our efforts to produce enhanced $YBa_2Cu_3O_{7-\delta}$-based J_c wire. Two subcontracts that were being negotiated last quarter were subject to the availability of funding. The first was with the HTSC Pilot Center at Oak Ridge National Laboratory is being renegotiated to focus the effort consistent with the new funding. This subcontract will be aimed at quantifying and improving the $YBa_2Cu_3O_{7-\delta}$ fiber melt-texturing process developed at CPS Superconductor. This Oak Ridge subcontract will give the program access to sophisticated analytical facilities and materials expertise that will greatly enhance our capabilities. The second subcontract that was under negotiation with the University of Michigan aimed at achieving an understanding of magnetic flux pinning in HTSC materials was abandoned.

We will continue to develop the continuous $YBa_2Cu_3O_{7-\delta}$ fiber melt-texturing process described in this report with our efforts focused primarily on studying the relationship between processing conditions, microstructure, and J_c. A primary concern is a definition of the parameters that limit the rate of the $YBa_2Cu_3O_{7-\delta}$ crystallization front progression, thus the conductor production rate. Our effort in this area will be substantially enhanced by our pending agreement with the Oak Ridge National Laboratory. A series of quench and polish experiments are underway to investigate microstructures that are "frozen" during the melt-processing. These experiments will allow us to examine the microstructures including the phase formation and grain morphology at critical positions and times during the process.

In addition, we will continue to place samples of this melt-textured fiber in the hands of potential users within the DARPA HTSC Initiative (for example, Boeing Aerospace, NIST-Boulder, Bio-Magnetic Technologies, General Electric and NIST-Gaithersburg. In addition, as part of an EPRI-sponsored program to develop HTSC underground power transmission cables, CPS Superconductor will supply 1 m samples of melt textured fiber Underground Systems, Inc. of Armonk, NY for evaluation including unique AC current and AC magnetic field characterization.

Work will also continue on melt-textured three-dimensional shape development, both to provide the active elements for our trapped flux motor, and to continue to provide samples for users within the DARPA HTSC Initiative (Boeing Aerospace and Mechanical Technologies). Efforts focus on the definition of the relationship between composition/processing and microstructure/ performance where the criteria for performance will be both macroscopic transport J_c around the circumference of a trapped flux motor magnet ring-replica, and magnetic flux trapping for other shapes. The flux trapping parameter is measured in-house using a newly acquired magnetic fluxmeter and sample jig designed at Emerson Electric.

We feel uniformity in our melt-textured bulk shapes will be greatly improved with the use of heat baffles presently being tested to produce a more truly isothermal environment. In an isothermal environment, nucleation and growth obeys the classic theory and occurs randomly allowing the entire sample to be melt-textured. The isothermal environment is currently being improved for the processing of the disks. In addition, the thermal gradient will be improved for both the fiber processing (by

designing a new furnace), and for the ring/disk processing by incorporating directional heat "source" (a "hot" plate in the furnace) or a heat "sink" (cool air directed over the bulk shape).

Additional fiber development we have planned throughout the remainder of the program includes combinations of several one meter long melt-processed fibers for evaluation. Also, small diameter coils ($\leq$ 1 cm diameter with $\leq$ 10 mil fiber) and multifilament braid, if available, will be tested using our melt-processing technique. The coil shapes will test certain physical limits of our process (i.e., temperature variations, shape retention, relative thermal gradient effects, and so on) as well as electromagnetic properties of small coils. The multifilament braid will also test limits of our process (for example, the total mass processed in relation to the diameter of the filaments and transit through the furnace) and allow higher critical currents in the final product.

We have a laboratory scale process improving with each "run", and development is underway to achieve a manufacturable process. As the process for producing melt-texture fiber is defined, the effort to further develop the process into a manufacturable process will be increased. Currently, we are investigating a process that will incorporate a custom-designed furnace that will process a monolayer-wrapped "spool" of a continuous prefired fiber. The heat source will be parallel to the axis of the "spool"; the bobbin will covered with a Nextel™ belt that travels through a set of rollers. In the time it takes to melt-texture a length of fiber about the circumference of the "spool" (one complete rotation), the whole length of wound

prefired fiber will be melt-processed. Of the many issues that must be addressed before the furnace is actually assembled, the most important is the microstructure of the fiber where the initial melt-processing meets the final as the spool completes its rotation. A series of experiments are planned to address this issue that include examining the composition of our melt-textured fiber along the axis of the fiber from the initial heating until cooled and fibers that were passed several times through temperatures above the peritectic. Additional experiments will include measuring mechanical properties of the prefired fiber to determine the diameter of the "spool" furnace, developing the spooling device to wind the prefired spool of fiber, and testing the type of heat source that will best serve the needs of melt-processing.

4. FINANCIAL STATUS

As of December 30, 1990, the project had not received its authorized $1,304,264.56 allocation required in FY91 to meet the contract target of $5,509,387.00. The parent company, Ceramics Process Systems, will continue to support this program allowing to bill against costs until the funds are released, which is expected in the near future. Work at the subcontractors to this program was temporarily halted pending release of funds.